Optimising NMR Spectroscopy through Method and Software Development

Jonathan Yong

University of Oxford

Contents

refsection:1

refsection:2

refsection:3

refsection:4

Chapter 4

NOAH

chpt:noah

This final—and long—chapter describes my work on *NOAH* (NMR by Ordered Acquisition using ^{1}H detection) *supersequences*, pulse sequences which record multiple 2D datasets (‘*modules*’) in the time required for one. This is an attractive NMR technique for several reasons: the time savings are clearly a key factor, but the flexibility of being able to combine almost any set of modules also makes NOAH supersequences applicable to a variety of contexts.

I begin by introducing the concepts underlying NOAH supersequences, as well as a general discussion of the time savings (and sensitivity per unit time) benefits thus realised. I then describe the GENESIS (GENEration of Supersequences In Silico) website, which allows users to generate Bruker pulse programmes for almost every imaginable NOAH supersequence. After this, my work on various aspects of the actual sequences themselves is described, with a special focus on newly developed and/or improved modules. Finally, the design of ‘parallel’ supersequences which use interleaved and/or time-shared modules is discussed.

This work was done in close collaboration with Ēriks Kupče (Bruker UK). However, all results and analysis shown in this chapter are mine. The work in this chapter forms the subject of several publications:

- Yong, J. R. J.; Hansen, A. L.; Kupče, Ē.; Claridge, T. D. W. Increasing sensitivity and versatility in NMR supersequences with new HSQC-based modules. *J. Magn. Reson.* **2021**, *329*, 107027, DOI: 10.1016/j.jmr.2021.107027
- Kupče, Ē.; Yong, J. R. J.; Widmalm, G.; Claridge, T. D. W. Parallel NMR Supersequences: Ten Spectra in a Single Measurement. *JACS Au* **2021**, *1*, 1892–1897, DOI: 10.1021/jacsau.1c00423
- Yong, J. R. J.; Kupče, Ē.; Claridge, T. D. W. Modular Pulse Program Generation for NMR Supersequences. *Anal. Chem.* **2022**, *94*, 2271–2278, DOI: 10.1021/acs.analchem.1c04

964

- Yong, J. R. J.; Kupče, Ē.; Claridge, T. D. W. Uniting Low- and High-Sensitivity Experiments through Generalised NMR Supersequences. **2022**, manuscript in preparation

The material in the introductory sections also closely follow two reviews which I have contributed to:

- Kupče, Ē.; Frydman, L.; Webb, A. G.; Yong, J. R. J.; Claridge, T. D. W. Parallel nuclear magnetic resonance spectroscopy. *Nat. Rev. Methods Primers* **2021**, *1*, No. 27, DOI: 10.1038/s43586-021-00024-3
- Yong, J. R. J.; Kupče, Ē.; Claridge, T. D. W. In *Fast 2D solution-state NMR: concepts and applications*, Giraudeau, P., Dumez, J.-N., Eds., forthcoming, 2022

4.1 Introduction

sec:noah__introduction

The characterisation of small molecules and biomolecules by NMR spectroscopy relies on a suite of standard 2D NMR experiments, which seek to detect heteronuclear scalar couplings (e.g. HSQC and HMBC), homonuclear scalar couplings (e.g. COSY and TOCSY), or through-space interactions (e.g. NOESY and ROESY). Although 2D experiments provide far superior resolution and information content compared to 1D spectra, they also require substantially longer experiment durations, as the indirect dimension must be constructed through the acquisition of many t_1 increments. This problem is further exacerbated by the fact that structural elucidation or verification often necessitates the acquisition of several different 2D experiments.

The acceleration of 2D NMR has thus proven to be a popular area of research. We may broadly categorise existing techniques into two classes: firstly, those which seek to directly speed up the acquisition of *individual* 2D spectra, and secondly, *multiple-FID* experiments which aim to collect two or more 2D spectra in the time required for one.* The former category includes methods such as non-uniform sampling (NUS),[7–10] fast pulsing (i.e. shortening of recovery delays),[11–14] ultrafast NMR,[5,15–19] Hadamard encoding,[20,21] and spectral aliasing;[22–24] whereas the latter encompasses time-shared NMR,[25,26] multiple-receiver NMR,[27–29] and—of course—NOAH supersequences.[5,30,31]

The scope of this introductory section will be limited to only NOAH supersequences. However, many of these techniques are closely related, and I will introduce concepts from elsewhere as needed. It should be noted that there are several other multiple-FID experiments which, while not explicitly advertised as such, are conceptually identical to NOAH experiments.[32–35] I do not discuss these here.

4.1.1 Time savings and sensitivity analyses

subsec:noah__snr

In a typical 2D NMR experiment, the majority of the experiment duration is taken up by the *recovery delay*—the time required for spins to return to their equilibrium polarisation, such that the next transient or t_1 increment can be recorded. The removal (or shortening) of recovery delays is thus a very effective way of speeding up 2D data acquisition. In NOAH supersequences, 2D experiments ('modules') can be directly concatenated without the addition of extra recovery delays between them: only one overall recovery delay is required for the entire supersequence. This means that, to a first approximation, a supersequence containing N modules ($N \geq 2$) can be acquired in the time needed for just one module. Figure 4.1 shows an example of a NOAH supersequence formed from two modules (HSQC and COSY): the various timings referred to in

*These are by no means mutually exclusive: many of the techniques here can be combined to provide even greater efficiency.

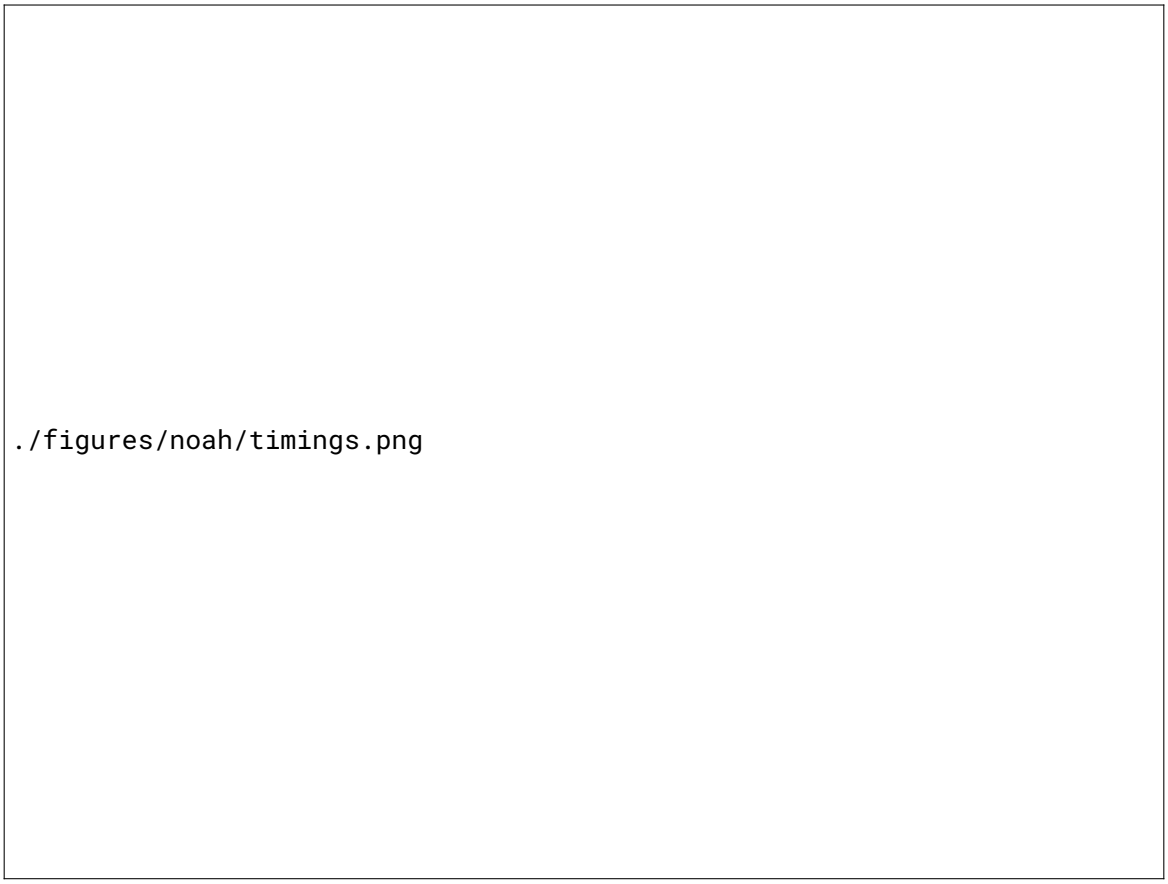

Figure 4.1: **(a)** NOAH-2 SC supersequence, comprising HSQC and COSY modules (see table 4.1 for an explanation of the single-letter module codes used). **(b)** 'Conventional' echo–antiecho HSQC (the same as in fig. 1.7). **(c)** 'Conventional' COSY. The timings referred to in the text are highlighted for all three experiments; I have assumed that d_1 for each experiment is the same. Note that the lengths are not to scale: d_1 is typically far longer than the τ_{ps} and τ_{acq}.

the text which follows are also marked on the diagram.

The duration of an NMR experiment, τ_{exp}, can be expressed as a sum of its parts:

$$\tau_{exp} = \tau_{ps} + \tau_{acq} + d_1, \tag{4.1}$$ {eq:exp_duration_2d}

where τ_{ps} is the time required for the pulse sequence itself (typically several milliseconds), τ_{acq} is the acquisition time (several hundred milliseconds), and d_1 is the recovery delay (one or more seconds). The *time-saving factor* ρ_t for a NOAH supersequence, as compared to a series of conventional standalone experiments, is then:

$$\rho_t = \frac{\sum_i \tau_{conv}^{(i)}}{\tau_{NOAH}} = \frac{\sum_i (\tau_{ps}^{(i)} + \tau_{acq}^{(i)} + d_1^{(i)})}{d_1 + \sum_i (\tau_{ps}^{(i)} + \tau_{acq}^{(i)})}, \tag{4.2}$$ {eq:rho_t}

where τ_{NOAH} is the duration of the NOAH experiment, τ_{conv} is the duration of a conventional

experiment, and the superscript (i) represents the i-th module or conventional experiment being acquired. The sum runs from $i = 1$ to N, where N is the number of modules. If we assume that $d_1^{(i)} = d_1$ is the same for all N conventional experiments and the supersequence, then in the limit where

$$d_1 \gg \sum_i \tau_{\text{ps}}^{(i)} + \tau_{\text{acq}}^{(i)}, \tag{4.3}$$ {eq:d1_limit}

we have that $\rho_t \to N d_1/d_1 = N$. This analysis makes plenty of assumptions, and is not entirely valid in practice. For example, *each* τ_{acq} is often around 5–10% of d_1, so is not entirely negligible, especially in longer supersequences. Furthermore, some modules require longer τ_{ps}: most notable is the NOESY module, which contains a mixing time of several hundred milliseconds. (HMBC, TOCSY, and ROESY spectra are also lesser offenders.) These factors serve to reduce ρ_t from its idealised value of N; generally, this deviation is larger as N increases, because eq. (4.3) becomes less and less valid. Nevertheless, the general point that time savings are approximately proportional to N stands.

For relatively concentrated samples, where sensitivity is not an issue, we can in fact end the discussion here. In this *sampling-limited regime*, the minimum 2D experiment duration is dictated purely by the number of t_1 increments needed to obtain sufficient resolution in the indirect dimension, as well as the minimum phase cycle required for artefact suppression.* NOAH supersequences are identical to conventional experiments in both aspects, but provide a time-saving factor of $\rho_t \sim N$.

The development of modern NMR instrumentation, including high-field magnets and cryogenic probes, means that the sampling-limited regime continues to be extended to ever lower concentrations. However, it is often not this simple: the opposite *sensitivity-limited regime* is still very commonly encountered, for example with naturally insensitive experiments (e.g. ADEQUATE), low-field benchtop NMR, or most simply, dilute samples.†

In such cases, it becomes mandatory to compare the SNRs of the NOAH modules and conventional experiments. To do so, we define for each module an *SNR factor* $A^{(i)}$, which is the SNR of the NOAH module divided by the SNR of a conventional experiment, acquired with the same parameters.‡ In general, we have that $A \leq 1$, because NOAH modules frequently contain small modifications from conventional experiments (as will be explained in § 4.1.2). The *gain in*

*With modern gradient-enhanced experiments, the minimum phase cycle may well not even be a 'cycle'; see also fig. 1.8.

†If the SNR factor $A^{(i)}$ as discussed below is *very small*, then it is possible that even concentrated samples may be shifted into the sensitivity-limited regime. This is never really the case in practice, though, as will be shown in § 4.1.3.

‡The relative SNR will likely vary from peak to peak in the spectrum, and $A^{(i)}$ should in theory be quoted either as an average over all peaks, or as a range. This is what I have done in this thesis. However, comparisons in the literature are not always as thorough.

sensitivity per unit time, $\varepsilon^{(i)}$, is then defined by

$$\varepsilon^{(i)} = A^{(i)}\sqrt{\rho_t}, \tag{4.4}$$ {eq:varepsilon_i}

where the square root accounts for the fact that SNR scales only as the square root of the number of scans, or the number of times the experiment can be repeated in a given period. Of course, the exact values calculated for $A^{(i)}$ (and hence $\varepsilon^{(i)}$) will depend on the sample chosen for the comparison. These values should therefore be assumed to be valid only for similar samples.

If $\varepsilon^{(i)} > 1$, as is frequently the case, this means that the NOAH supersequence provides greater sensitivity per unit time in the i-th module compared to a standalone experiment. Equivalently, performing a NOAH experiment allows data of sufficient sensitivity to be obtained in less time. Naturally, this condition is most important for modules which are inherently insensitive, particularly heteronuclear correlation modules. For sensitive (typically homonuclear) modules, it is often perfectly tolerable to have $A < 1$ or even $\varepsilon < 1$, as even with this sensitivity penalty they are still more intense than the heteronuclear modules.

Another issue with NOAH supersequences is that each module is run with the same number of scans (phase cycle). Although this was touted as a benefit in the sampling-limited regime, this may in fact be undesirable in the sensitivity-limited regime, where insensitive experiments need to be run with more scans than sensitive ones. In this case, the *effective* time savings provided by NOAH experiments are smaller:

$$\rho_{t,\mathrm{eff}} = \frac{\sum_i \tau_{\mathrm{conv}}^{(i)}}{\tau_{\mathrm{NOAH}}} = \frac{\sum_i S^{(i)}(\tau_{\mathrm{ps}}^{(i)} + \tau_{\mathrm{acq}}^{(i)} + d_1^{(i)})}{Sd_1 + S\sum_i(\tau_{\mathrm{ps}}^{(i)} + \tau_{\mathrm{acq}}^{(i)})}, \tag{4.5}$$ {eq:rho_t_eff}

where each standalone experiment is acquired with $S^{(i)}$ scans and the NOAH experiment with S scans. Typically, S is simply the largest of the $S^{(i)}$. If $S^{(i)} = S$ for all i, then eq. (4.5) simply reduces to eq. (4.2); on the other hand, if the $S^{(i)}$'s are different, then we have that $\rho_{t,\mathrm{eff}} < \rho_t$. In such a situation, it is probably more appropriate to describe a NOAH supersequence as 'measuring the most insensitive module and getting the others for free'. Indeed, if $S = S^{(i)} \gg S^{(j\neq i)}$, then 'the other' modules require almost no time to measure (relative to the least sensitive module), and $\rho_{t,\mathrm{eff}}$ tends towards 1, meaning that even the time-saving utility of NOAH vanishes. A corollary of this is that NOAH supersequences are generally best constructed from modules which have similar intrinsic sensitivities and hence similar $S^{(i)}$'s.

As the reader can no doubt appreciate by now, the comparison of NOAH and conventional spectra is fraught with subtleties (which are sometimes glossed over in the literature, but invariably surface in real-life discussions). In fact, it is hardly even difficult to construct yet more edge cases. For example, one may not want to acquire all the individual spectra 'conventionally': for example,

NUS may be used for a HSQC experiment but not for others; or d_1 may be varied for different experiments. These will have an impact on both the durations of the experiments, as well as their sensitivities. To make any meaningful quantitative comparisons, it is therefore necessary to restrict the discussion to values of ρ_t, A, and ε, which can be objectively calculated. This is the approach I have taken in this thesis. These should of course be read with the qualitative understanding that depending on the context, these aforementioned factors may lead to *some*—but never a *complete*—decrease in the utility of NOAH experiments.

4.1.2 Magnetisation pools

subsec:noah__magpools

Having gotten this relatively dry material out of the way, I now turn to exactly how NOAH supersequences are constructed. Ordinarily, if the recovery delay is removed from an NMR experiment, its sensitivity will be greatly reduced because insufficient magnetisation will have recovered between repetitions; or in other words, $A^{(i)}$ will be very small. Such experiments would only really be useful well in the sampling-limited regime.

The key to avoiding this in NOAH supersequences is to make sure that *each module samples a different source of magnetisation*. For example, a HSQC module can be designed to only sample magnetisation of protons directly bonded to the 1.1%-natural abundance ^{13}C, and leave all other proton magnetisation untouched. Immediately following this, the remainder of the proton magnetisation can then be used to record (say) a COSY module, without needing a separate recovery delay. Using the notation of Orts and Gossert,[36] the magnetisation of ^{13}C–bound protons is denoted as $^1\mathrm{H}^{\mathrm{C}}$, and the magnetisation of protons *not* bonded to ^{13}C is denoted as $^1\mathrm{H}^{!\mathrm{C}}$. Protons not directly bonded to NMR-active heteronuclei are labelled $^1\mathrm{H}^{!\mathrm{X}}$, and will often be referred to as 'bulk' magnetisation, since (in natural-abundance samples) the majority of protons fall into this category.

Most standard 2D experiments do not preserve unused magnetisation but instead dephase it through CTP gradient selection; thus, NOAH modules often require some modifications compared to standard experiments. For example, compared to the echo–antiecho HSQC (discussed in § 1.4.5), the NOAH HSQC module[30] adds an extra CTP gradient so that the bulk magnetisation is refocused and ultimately returned to the $+z$ equilibrium state (fig. 4.2a). (This is largely identical to the 'symmetrised' ASAP-HSQC experiment.[37])

Sometimes, the modifications required are more extensive, as in the HMBC module. If this module is followed by a HSQC module (or any other module which draws on $^1\mathrm{H}^{\mathrm{C}}$ magnetisation), the initial 90° excitation pulse must be replaced with a zz-filter (fig. 4.2b). This performs an *isotope-selective rotation* in that $^1\mathrm{H}^{\mathrm{C}}$ magnetisation is stored along the z-axis, but $^1\mathrm{H}^{!\mathrm{C}}$ magnetisation is excited (and subsequently detected). In general, sequences which are thus modified have lower

figure.caption.4

Figure 4.2: **(a)** NOAH HSQC module. **(b)** NOAH HMBC module. The 90° pulse highlighted in red is described in § 4.3.7. Delays are set as: $\Delta = 1/(4 \cdot {}^{1}J_{\mathrm{CH}})$; $\Delta_{\mathrm{LR}} = 1/(2 \cdot {}^{n}J_{\mathrm{CH}})$; $\tau_1 = 1/(2 \cdot {}^{1}J_{\mathrm{CH,max}})$; $\tau_2 = 1/(2 \cdot {}^{1}J_{\mathrm{CH,min}})$ (see also § 3.4.7 for the LPJF). Phase cycling is performed with $\phi_1 = (x, -x)$, $\phi_2 = (x, x, -x, -x)$, and $\phi_{\mathrm{rec}} = (x, -x, -x, x)$. Gradient amplitudes are $(g_1, g_2, g_3, g_4, g_5) = (80\%, \pm 40.2\%, 15\%, -10\%, -5\%)$. Product operator analysis is provided above both modules for both the ${}^{1}\mathrm{H}^{\mathrm{C}}$ and ${}^{1}\mathrm{H}^{!\mathrm{C}}$ magnetisation pools; the notation for this is explained in the *Preface*.

sensitivities (i.e. $A < 1$) than the 'original' sequences from which they were derived. This is partly because of imperfect manipulation of magnetisation by the extra pulse sequence elements, and also increased losses due to relaxation during these extended sequences.

In contrast, modules placed towards the *end* of a supersequence do not need to be modified, as they do not need to preserve any magnetisation. This includes virtually all homonuclear modules, which are allowed to simply consume any remaining magnetisation. Although this makes their implementation very straightforward, in general these modules will *also* suffer some losses in sensitivity, because the preceding modules do not perfectly retain all magnetisation.

Thus, in general, it is not possible for any module in a NOAH supersequence to have $A = 1$,

unless it is placed first in the supersequence *and* has not undergone any modifications.* Such cases are very rare, and it is thus necessary to accept some decreases in A, which are often fairly small (on the order of 10–20%). In the sampling-limited regime, sensitivity is not at a premium and this is often perfectly tolerable. In the sensitivity-limited regime, the full time savings ρ_t cannot be realised, but since ε is still typically larger than 1, there is still an overall boost in sensitivity per unit time.

4.1.3 Case studies

sec:noah__case_studies

Using all that has been described in the previous sections, we now look at a few 'typical' supersequences to understand their construction. A quick note about the nomenclature of NOAH supersequences is warranted here. Supersequences are labelled by the number of modules N, plus a series of single-letter codes corresponding to the identity and ordering of the modules involved (table 4.1). Occasionally, superscripts or subscripts are used to qualify the modules involved.† Thus, a NOAH supersequence containing three modules—say ^{15}N HMQC, ^{13}C HSQC, and CLIP-COSY—would be referred to as a NOAH-3 $\mathrm{M_N SC^c}$. Table 4.2 provides values of ρ_t and A for each module of several typical supersequences, which will be rationalised in the text which follows.

NOAH-2 SC: HSQC + COSY

We begin with perhaps the simplest example of a NOAH supersequence, one containing the HSQC and COSY modules: this is labelled as a NOAH-2 SC experiment (entry 1, table 4.2). As shown in fig. 4.2a, the HSQC module only samples $^1\mathrm{H}^\mathrm{C}$ magnetisation, and leaves $^1\mathrm{H}^{!\mathrm{C}}$ magnetisation along the $+z$-axis Although the HSQC experiment has to be modified to preserve this $^1\mathrm{H}^{!\mathrm{C}}$ magnetisation, its sensitivity is practically unaffected as compared to a 'standard' HSQC ($A = 0.97$). Furthermore, the COSY module retains *most* of its sensitivity ($A = 0.90$). The small loss here is because the HSQC module does not *perfectly* preserve the $^1\mathrm{H}^{!\mathrm{C}}$ magnetisation: for example, evolution of J-couplings as well as relaxation occur during the HSQC pulse sequence, which are ignored in the product operator analysis in fig. 4.2a.

The value of the time-saving factor, $\rho_t = 1.87$, is very close to the theoretical limit of $N = 2$. This reflects the fact that the pulse sequence itself, τ_{ps}, is fairly short for both the HSQC and COSY

*Of course, this also depends on exactly *what* standalone experiment the NOAH supersequence is being compared against. Sometimes, in the literature, the NOAH experiment has been compared against its constituent modules acquired in a standalone fashion; in this case, the first module will always have $A = 1$. This tells us how much we gain through the act of concatenating modules, but is less meaningful in the 'real world' where one is interested in how useful NOAH is relative to 'typical' optimised 2D experiments. I therefore prefer to make comparisons against standard-library sequences.

†With the increasing number of modules, and the variety of modern NMR experiments which could be incorporated into NOAH supersequences, keeping these abbreviations short yet meaningful has been a challenge.

^{1}H–^{15}N modules		^{1}H–^{13}C modules		^{1}H–^{1}H modules	
Module	Code	Module	Code	Module	Code
HMQC	M_N	HSQC	S	COSY	C
HSQC	S_N	seHSQC	S^+	CLIP-COSY	C^c
seHSQC	S_N^+	HSQC-TOCSY	S^T	DQF-COSY	C
HMBC	B_N	HSQC-COSY	S^C	TOCSY	T
		2BOB	O	NOESY	N
		HMBC	B	ROESY	R
		ADEQUATE	A	PSYCHE	P
				TSE-PSYCHE	P^T
				PSYCHE 2DJ	J

tbl:noah_modules

Table 4.1: A (non-exhaustive) list of single-letter module codes for a selection of NOAH modules. Note that, in the literature, the ^{15}N HMQC module has been referred to simply by 'M', since the HSQC module is preferred for ^{1}H–^{13}C correlations. In this thesis, I include the subscript N throughout to avoid any ambiguity.

Entry	Sequence	τ_{NOAH}	ρ_t	A				
				HMBC	seHSQC	HSQC	COSY	TOCSY
1	SC	15 min 0 s	1.87			0.97	0.90	
2	SCT	16 min 25 s	2.60			1.01	0.99	0.79
3	BS	15 min 40 s	1.82	0.93		0.87		
4	SB	15 min 35 s	1.83	0.99		0.96		
5	BSCT	17 min 48 s	3.22	0.95		0.90	0.36	0.28
6	BS_N^+CT	18 min 57 s	3.74	0.95	0.71	0.66	0.38	0.30
7	S_N^+BSCT	18 min 56 s	3.75	0.76	0.79	0.74	0.33	0.26

tbl:noah_sensitivities

Table 4.2: Sensitivity and time-saving analyses of several typical NOAH supersequences. All experiments were acquired with 2 scans per increment, 256 t_1 increments, an acquisition time of 67 ms, and a recovery delay of 1.5 s. The HMBC module used here includes the extra ^{13}C 90° pulse described later in § 4.3.7: this has no significant impact on the SNR, and is only mentioned as a technicality. The ^{15}N seHSQC module is that described in § 4.3.2. The CT module here was run with States indirect-dimension quadrature detection, and the individual C module (in entry 1) with echo–antiecho. The following Bruker library sequences were used as the 'conventional' experiments: `hmbcetgpl2nd`, `hsqcetf3gpsi2`, `hsqcetgpsp.2`, `cosygpqf`, and `dipsi2gpphzs`. *Data code:* `7Z-220224`.

modules; the deviation therefore chiefly arises from the acquisition time, τ_{acq}. In all respects, this is therefore an example of an 'ideal' NOAH supersequence, where the combination of two modules provides time savings without compromising on sensitivity.

It is worth pointing out that the order of the modules cannot be reversed: the COSY module cannot be (easily) modified to preserve $^1H^C$ magnetisation. In a hypothetical NOAH-2 CS supersequence, the later HSQC module would only be able to use magnetisation recovered

during the COSY FID, leading to substantial sensitivity drops.

sc_noah_vs_conv_negative

Figure 4.3: **(a)** HSQC from NOAH-2 SC supersequence. **(b)** COSY from NOAH-2 SC supersequence. **(c)** Standalone HSQC. **(d)** Standalone COSY; off-diagonal artefacts are highlighted in the red box. *Data code:* `7Z-220224`.

A final point to consider would be whether the NOAH data has comparable spectral quality in terms of (for example) artefacts. In this case, the answer is yes: the NOAH HSQC spectrum is virtually identical to the standalone (figs. 4.3a and 4.3c; both spectra have low-level artefacts of different kinds, which do not seriously impede the interpretation and are not shown). On the other hand, the NOAH COSY spectrum seems to actually *improve* on the standalone COSY, in that it better suppresses off-diagonal artefacts (figs. 4.3b and 4.3d). These artefacts likely arise in the standalone COSY because of accidental refocusing of magnetisation which has not completely relaxed between t_1 increments.[38] In contrast, the NOAH COSY module has an extra set of HSQC gradients between every repetition of the COSY, so accidental refocusing is less likely. (Similar artefacts have been noted before in the DQF-COSY experiment,[39,40] and have also shown to

be attenuated in the corresponding NOAH module.[41]) That said, such improvements are not always guaranteed: there are sometimes artefacts which arise uniquely in NOAH experiments, some of which are discussed in the following sections.

NOAH-3 SCT: HSQC + COSY + TOCSY

Evidently, the fact that the HSQC preserves almost all $^{1}H^{!C}$ magnetisation means that *any* homonuclear module—or a combination thereof—can be placed after it. In general, since homonuclear modules tend to consume any remaining bulk magnetisation, it is very difficult to create combinations of homonuclear modules which do not lead to significant reductions in sensitivity. The only real exceptions are COSY/X combinations, where X can be NOESY, ROESY, or TOCSY: instead of concatenating the COSY and X modules, the COSY pulse sequence can instead be nested *within* the X module, as was first demonstrated with X = NOESY.[42,43] Here, we use the COSY/TOCSY combination as an example.[44] The COSY, TOCSY, and combined COSY/TOCSY modules are shown in fig. 4.4.

Figure 4.4: **(a)** COSY module. **(b)** TOCSY module; zero-quantum suppression is employed before and after the isotropic mixing period. **(c)** Combined COSY/TOCSY module, where the COSY FID is acquired immediately before the TOCSY mixing.

As shown in table 4.2 (entry 2), this nesting of the COSY module does not materially affect the TOCSY sensitivity. A small loss of approximately 20% is observed, which is partly due to the imperfect magnetisation preservation by the HSQC, and perhaps also due to relaxation during the COSY acquisition period. As for the time-saving factor, a slightly larger deviation ($\rho_t = 2.60$) is observed from the ideal value of 3. This reflects the addition of a TOCSY mixing period, which contributes to τ_{ps}.

NOAH-2 BS: HMBC + HSQC

As mentioned previously, the HMBC module shown in fig. 4.2b is designed to retain $^{1}H^{C}$ magnetisation through the addition of the *zz*-filter. This can be used in a subsequent HSQC module in a NOAH-2 BS supersequence. Entry 3 of table 4.2 shows that the addition of the

zz-filter to the HMBC causes a relatively small 7% decrease in sensitivity; on the other hand, the HSQC loses 13% of its sensitivity because of incomplete magnetisation preservation.

Generally, it has been recommended that less sensitive modules are placed earlier in the supersequence so that they can access a larger proportion of the equilibrium magnetisation. Since the HMBC is less sensitive of the two modules, this rule of thumb suggests that the BS supersequence would be better than the alternative SB supersequence. In fact, the opposite is true, as entry 4 of table 4.2 shows. The HSQC module has a boost in sensitivity because it is placed first in the supersequence, and no longer needs to rely on the $^{1}H^{C}$ magnetisation preserved by the HMBC; and the HMBC also benefits because the *zz*-filter modification is no longer needed.* Arguably, the ordering of modules in a supersequence should be considered on a case-by-case basis.

NOAH-4 BSCT: HMBC + HSQC + COSY + TOCSY

We now move on to a longer supersequence containing four modules, with a correspondingly larger ρ_t value of 3.22. The sensitivity of the HSQC module is practically the same as in the NOAH-2 BS supersequence just described: however, the COSY and TOCSY modules expose one weakness of the HMBC module which has so far been overlooked. In principle, the HMBC module should only excite magnetisation of protons which are long-range coupled to ^{13}C (which we could, for example, denote as $^{1}H^{C(LR)}$). This magnetisation pool should be separate from both the directly coupled protons ($^{1}H^{C}$), as well as protons which are not coupled to any ^{13}C at all ($^{1}H^{!C}$). Unfortunately, this is not the case: it is not actually possible to separate the $^{1}H^{C(LR)}$ and $^{1}H^{!C}$ magnetisation pools. The HMBC excites both of these magnetisation sources, dephases the latter using CTP gradients, and detects the signal arising from the former.

What this means, of course, is that the COSY/TOCSY module which rely on $^{1}H^{!C}$ magnetisation will have substantially lower sensitivities. The signal detected in these two modules derives only from whatever has recovered during the previous two acquisition periods, as shown in entry 5 of table 4.2: A for COSY and TOCSY is 0.36 and 0.28 respectively. That said, this is in fact not likely to be an issue *even* for sensitivity-limited samples. Because the intrinsic sensitivity of the HMBC is orders of magnitude lower than the COSY and TOCSY, even with these large losses in sensitivity, the COSY and TOCSY spectra still have greater intensities than the HMBC. Thus, as long as the entire supersequence is acquired with enough scans to make the HMBC SNR sufficient, the SNR in the COSY and TOCSY will *also* be acceptable. This is illustrated in fig. 4.5.

A rather more insidious problem is that different signals relax at different rates: thus, the COSY and TOCSY spectra (or indeed, any homonuclear module) will have uneven intensities and are

*In fact, the final 180° pulse in the HMBC module could also be removed: this is likely to give a further boost in SNR, as discussed in § 4.3.7. However, this was not done here.

frequently asymmetric. This can be seen in the COSY spectrum, where a pair of asymmetric crosspeaks are highlighted. Adding a period of isotropic mixing before the COSY module[45] can help to ameliorate this to some extent (this was not performed when acquiring the data in fig. 4.5).

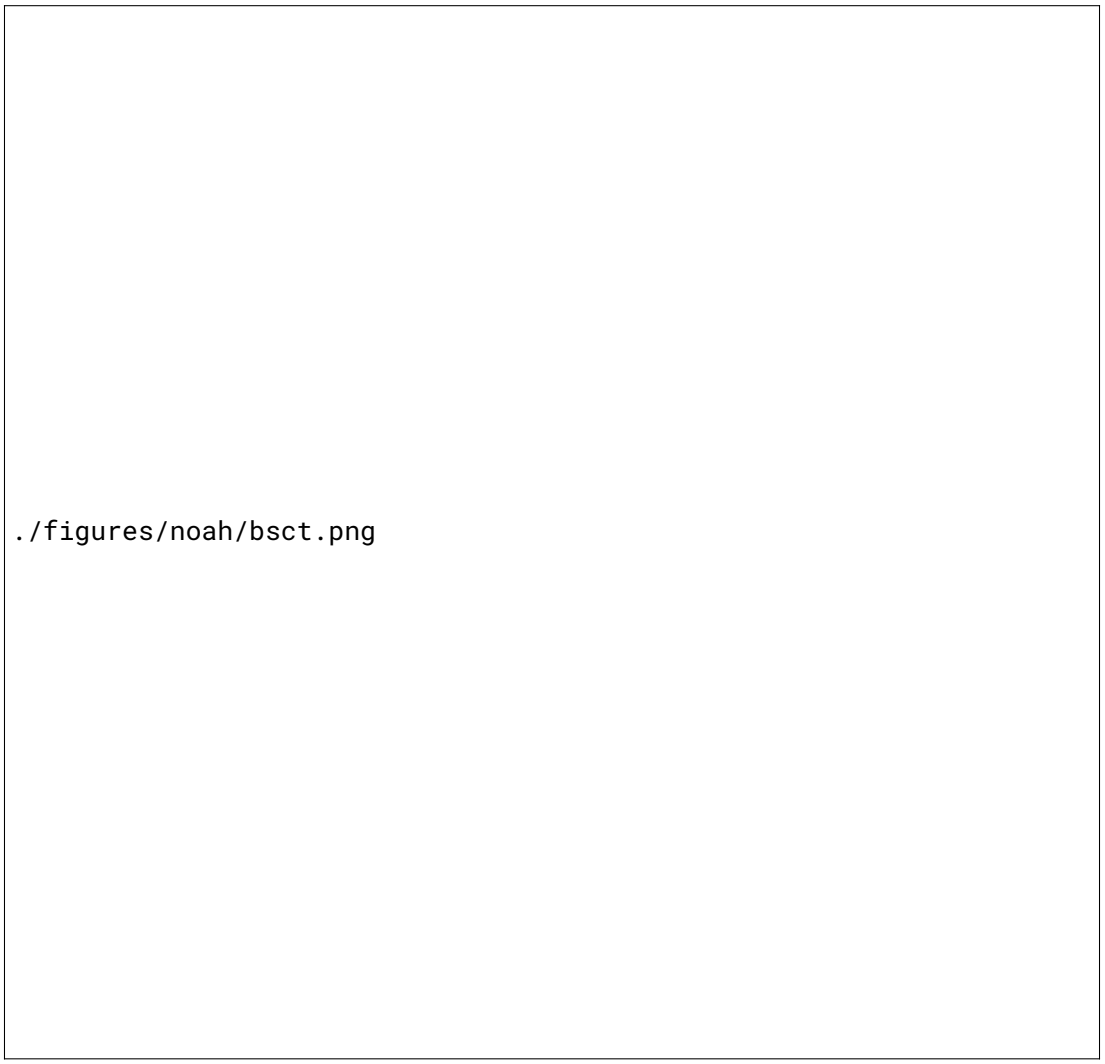

fig:bsct

Figure 4.5: Spectra obtained from a NOAH-4 BSCT supersequence. **(a)** HMBC. **(b)** HSQC. **(c)** COSY; a pair of asymmetric crosspeaks are highlighted with red arrows. **(d)** TOCSY (60 ms DIPSI-2 mixing). Despite the COSY and TOCSY having only ~ 30% sensitivity compared to standalone experiments, the intensity of the spectra obtained is still perfectly acceptable (the contour levels chosen are 1–2 orders of magnitude larger than for the HMBC). *Data code:* `7Z-220224`.

NOAH-5 BS$^{+}_{N}$SCT: HMBC + ^{15}N seHSQC + HSQC + COSY + TOCSY

As the final example, we add a further magnetisation pool to the mix, namely protons directly coupled to ^{15}N (i.e. $^{1}H^{N}$). As of the time of writing, the implementation of multiple-FID experiments on Bruker spectrometers limits N to a maximum of 5, so a supersequence such as

the present NOAH-5 $BS^{+}_{N}SCT$ is the current limit. (However, there is no *scientific* argument forbidding $N > 5$, and it is likely that in future versions of TopSpin this restriction will be lifted.)

The values of A for each module are given in entry 6 of table 4.2. If the HMBC module is placed at the beginning of the supersequence, then in order to preserve *both* $^{1}H^{N}$ and $^{1}H^{C}$ magnetisation, the zz-filter must be extended to include ^{15}N pulses.[46] As before, the ^{15}N seHSQC and ^{13}C HSQC modules both suffer drops in sensitivity. For the ^{15}N seHSQC, this is partly because of imperfect preservation of $^{1}H^{N}$ magnetisation by the HMBC, but also stems from the addition of the zz isotope-selective pulse (ZIP) element to the seHSQC pulse sequence; this is described further in § 4.3.2. On the other hand, for the ^{13}C HSQC, the sensitivity loss stems purely from imperfect retention of $^{1}H^{C}$ magnetisation. Finally, because the HMBC dephases $^{1}H^{!X}$ magnetisation, the COSY and TOCSY at the end have lower sensitivities: however, as discussed above, this is not an issue in practice.

It is also possible to move the ^{15}N seHSQC module to the front: this gives it a slightly greater sensitivity, at the cost of the HMBC (entry 7, table 4.2). In general, these two modules tend to have comparable sensitivity, and which of these two arrangements is better depends on which module the sensitivity needs to be optimised for.

Lastly, the value of ρ_t given here of 3.74 represents an effective upper limit on the time-saving factor. Although ρ_t increases with N, the extent to which it deviates from the ideal value of N also increases: it is very difficult to obtain $\rho_t > 4$, even with five modules in the supersequence. Of course, it is possible to increase ρ_t further by lengthening the recovery delay d_1 used for the experiments: for example, if d_1 is increased to 2 s from its present value of 1.5 s, ρ_t increases to 3.94. Obviously, this can only be pushed so far before it becomes meaningless.

4.2 GENESIS: automated pulse programme creation

sec:noah__genesis

In this section, I discuss the development of the GENESIS (GENEration of Supersequences In Silico) website (fig. 4.6): as the name suggests, it automatically generates pulse programmes for arbitrary NOAH supersequences. The website also provides extensive instructions on acquiring and processing NOAH data. Although this may at first glance appear slightly out of chronological order, in that the paper[3] was published later than much of the other work in this chapter, an early version of the GENESIS tool was in fact created much earlier (by July 2020).

The present version of GENESIS is available at `https://nmr-genesis.co.uk`; the source code can also be obtained from `https://github.com/yongrenjie/genesis`.

fig:genesis_frontpage

Figure 4.6: The front page of the GENESIS website (https://nmr-genesis.co.uk), as of 10 September 2022.

4.2.1 Motivation

ah__genesis_motivation

From the preceding discussion in § 4.1, it is clear that modules which use different magnetisation pools can be combined almost at will. It does not matter *what* modules they are, merely what magnetisation pools they consume (and preserve). Thus, for example, the NOAH-2 SC supersequence can in fact be generalised to any $^{1}H^{C}$ module plus any $^{1}H^{!C}$ module. Very broadly speaking, we may define a generic supersequence as having any or all of the following:

- a HMBC module, which actually uses $^{1}H^{!X}$ magnetisation but can be placed at the front as discussed in the NOAH-3 BSC example above;
- a $^{1}H^{N}$ module;
- one or more $^{1}H^{C}$ modules (it is possible to partition the $^{1}H^{C}$ magnetisation pool between two modules, as will be discussed in § 4.3.4);
- one or more $^{1}H^{!X}$ modules which consume bulk magnetisation.

In the first NOAH paper in 2017,[30] a total of 285 'viable' supersequences were already listed. If we further take into account some of the new modules which were developed over the course of my DPhil (§ 4.3), the generic formula above provides for over 4000 viable supersequences.*

*This is also ignoring the 'parallel' supersequences, which are discussed in § 4.5. The support for parallel supersequences in GENESIS is not complete: integrating these fully would require substantial changes to the user interface, which I have not had time to do.

('Non-viable' sequences would be those which have undesirable drawbacks: for example, wrongly ordered modules like in a NOAH-2 CS supersequence.)

In spite of this, *only around 45 pulse programmes* had been made available (either via the supplementary information of NOAH papers, or the Bruker User Library). Traditionally, pulse programmes must be written by hand, which is a laborious and fairly error-prone process made worse by the sheer length of NOAH experiments. Doing this for thousands of supersequence is clearly impractical; furthermore, each time a new module is developed, or an old module is improved, updating every relevant supersequence would itself already be a mammoth task. This explains why—although the NOAH concept provides a clear blueprint for how supersequences may be constructed—there is still a huge gap between theory and practice.

To bridge this gap, I turned towards the *programmatic* generation of pulse programmes.* This not only allows for existing supersequences to be generated at will, but also provides an easy way for updates to be rapidly disseminated to the NMR community. Furthermore, a website can serve as a 'one-stop' shop where—after downloading pulse programmes—users may download the associated NOAH processing scripts and also access instructions on how to run NOAH experiments. This information did already exist, but was scattered across several different websites and/or journal supplementary information documents, and would have been needlessly confusing to a new user (not to mention the different versions of scripts available in different publications).

4.2.2 Implementation details

genesis_implementation

I will now describe a few features of GENESIS pulse programmes, as well as how these are implemented. The GENESIS code is written in TypeScript; during deployment, this is compiled to JavaScript, which can then be directly executed in the client's web browser. No server-side code is required, meaning that the GENESIS web page is actually a static site (it is currently hosted using GitHub Pages).

Overall structure

The algorithm used for pulse programme construction can loosely be separated into three parts, which are shown in listing 4.1:

1. the *preamble*, which consists of everything up until the beginning of the actual pulse sequence (the `ze` command). This includes header comments as well as definitions of

*This is actually a bit of a lie: GENESIS was initially created for my own convenience. Throughout this chapter, I have had to perform many comparisons of different supersequences, and this tool spared me from having to write everything by hand (and—more often than not—subsequently discover mistakes which invalidated the results). Of course, it soon became apparent that it could find much wider use.

```
/* PREAMBLE */
; gns_noah2-SCqf
; 13C HSQC
; 1H magnitude-mode COSY
"d4          = 0.25s/cnst2"  ; 13C INEPT
"in0         = inf1/2"       ; 13C HSQC increment
"in11        = 2*dw"         ; COSY increment
; ...
define delay DC_HSQCa
"DC_HSQCa    = d4-p14/2"
"l0          = td1/2"        ; TD1/NBL

/* MAIN SECTION */
1 ze
4 d1 st0
  ; MODULE 1 - HSQC
  (p1 ph0):f1
  ; ...
  goscnp ph30 cpd2:f2
  50u do:f2
  2m st
  ; MODULE 2 - COSY
  (p1 ph12):f1
  ; ...
  go=2 ph26
  1m iu1        ; TD1/NBL counter
  1m igrad EA   ; echo-antiecho gradients
  1m id11       ; COSY t1
  30m wr #0 if #0 zd
if "l1 % 2 == 0" {
  1m id0        ; HSQC t1
}
  lo to 4 times l0
exit

/* EPILOGUE */
ph0=0
;gpnam4: SMSQ10.100
;gpz4: 70% (13C CTP)
;cpd2:wvm:wudec: cawurst_d-20(220 ppm, 1.4 ms; L2H)
;d4: 1/4J(CH)
;auprog: noah_hsqc:noah_cosy QF
;module identifiers: C_HSQC H_COSY_QF
;pulse programme created by genesis-v2.2.2, https://nmr-genesis.co.uk
;Sun Sep 11 2022 16:04:54 GMT+0800 (Malaysia Time)
```

Listing 4.1: Abridged GENESIS pulse programme for the NOAH-2 SC supersequence shown in fig. 4.1a.

lst:genesis_sc

parameters, such as delays and pulse widths;

2. the *main section*, which contains the actual pulse sequence;
3. the *epilogue*, which contains phase cycle information as well as footer comments describing each parameter. Instructions for generating shaped pulses using Bruker's WaveMaker software are also included here, as well as instructions for automatic processing (§ 4.2.3), and comments indicating how the pulse programme was generated (for reproducibility purposes).

The construction of the preamble and main section is largely accomplished through the collation of module-specific information, the most important of which are:

- information about the module itself, which go into the header comments;
- parameter definitions, which are collated to form the preamble. Duplicates must be removed here to avoid errors; and
- the pulse programmes themselves, which are directly concatenated to form the main section.

These, as well as other smaller bits of information (e.g. relevant citations, appropriate processing scripts), are stored within `NOAHModule` objects (an example is provided in listing 4.2). Each distinct module corresponds to one such object. Therefore, if one wants to add a new module to GENESIS, most of the work can be completed by simply defining a new `NOAHModule` object: no changes to the algorithm itself are needed.

To put the epilogue together, the pulse programme constructed so far is scanned for pulse phases, shaped pulses, and all other parameters. Using predefined lookup tables, GENESIS then outputs pulse phase definitions, WaveMaker directives (where appropriate), and comments containing textual descriptions of each parameter. These comments are mostly cosmetic, but are very useful to the user as they are displayed in the `ased` screen when setting up an experiment. Finally, instructions for automatic processing of the NOAH data (explained in § 4.2.1) are added to the bottom, together with the version number and a timestamp (for reproducibility purposes).

Phase/delay incrementation and looping

Since NOAH experiments are 2D experiments, there is one additional complication: the pulse programme must contain appropriate looping statements, together with pulse phase and delay incrementation, in order to correctly generate the indirect dimension. In many existing NOAH pulse programmes, looping in 2D experiments was written using the equivalent of `for` loops (listing 4.3, *left*). Although this suffices for the vast majority of supersequences, whenever anything must be incremented in a different way (e.g. for parallel supersequences, or the PSYCHE module

```
let shortDescription = `; 13C HSQC`

let preamble = `
"d4      = 0.25s/cnst2"                ; 13C INEPT
; ...
"D[ID]a  = d4-p14/2"    // [ID] is later replaced with the module code
`

let pulprog = `
  ; 13C-1H HSQC

  ; INEPT
  (p1 ph0):f1
  ; ...
  goscnp ph30 cpd2:f2
  50u do:f2
`

const mod = new NOAHModule(
    "C_HSQC",           // internal module code
    "c13",              // module category
    "S",                // single-letter code, Table 4.1
    [],                 // relevant citations (if any)
    "noah_hsqc",        // AU programme for processing
    shortDescription,   // short description
    [AF_EDIT],          // available acquisition flags
    preamble,           // preamble text
    pulprog,            // pulse programme text
    1,                  // number of FIDs
    false               // flag for 'parallel' modules
);
export default mod;
```

Listing 4.2: An excerpt of the `NOAHModule` object for the HSQC module (internal code `C_HSQC`.

lst:module_c_hsqc

which uses a different number of t_1 increments), the nested loop structure must be modified. I therefore opted to change the structure to use only one loop, and to control the phase and delay incrementation using modular arithmetic (listing 4.3, *right*). The outcome is entirely equivalent, but edge cases can be implemented simply by adding another check on the loop counter `L1`.

Parameter standardisation

Each NOAH module contains a number of parameters, including pulse widths, delays, gradient amplitudes, shaped pulse waveforms. Since different modules are stored separately (as differ-

```
"l0 = td1/4"


1 ze
3 1m
4 d1 st0

  ; ... (pulse sequence goes here)

  ; in inner loop
  1m igrad EA   ; HSQC gradients
  1m id11       ; COSY t1
  30m wr #0 if #0 zd
  lo to 4 times 2

  ; in outer loop
  1m ip5*2      ; HSQC 13C 90
  1m ip30*2     ; HSQC receiver
  1m id0        ; HSQC t1
  lo to 3 times l0



end
```

```
"l0 = td1/2"
"l1 = 0"

1 ze
4 d1 st0


  ; ... (pulse sequence goes here)

  ; on every pass
  1m iu1        ; loop counter
  1m igrad EA   ; HSQC gradients
  1m id11       ; COSY t1
  30m wr #0 if #0 zd

  ; on every second pass
  if "l1 % 2 == 0" {
    1m ip5*2      ; HSQC 13C 90
    1m ip30*2     ; HSQC receiver
    1m id0        ; HSQC t1
  }
  lo to 4 times l0

end
```

Listing 4.3: Implementation of phase/delay incrementation and looping in previous NOAH sequences (*left*, using nested loops) and in GENESIS (*right*, using modular arithmetic).

lst:genesis_looping

ent objects), directly concatenating their pulse programmes may lead to conflicting parameter definitions. GENESIS avoids this by maintaining a global table of parameter definitions which are applied to all modules: when new modules are added, they must be checked against this to ensure that there are no inconsistencies.

In general, where possible, these parameters are chosen to be consistent with pulse programmes in the Bruker standard library: thus, for example, `P1` is the ^{1}H 90° pulse width, and `CNST2` is the $^{1}J_{\mathrm{CH}}$ value used for calculating INEPT delays. This makes it easy to read in parameters either from the *prosol* relation tables in TopSpin, or from other existing parameter sets. Some delays are module-specific and do not need to be reused, and in standard library sequences, are often labelled as `DELTA1`, `DELTA2`, and so on. To avoid conflicting definitions and also to improve readability, I rename these such that they include the name of the module: thus, in a ^{13}C HSQC these may be labelled `DC_HSQC_1`. Here, `C_HSQC` is the name associated with the `NOAHModule` object.

If combined with some caution when adding new modules, these measures ensure that *within* a supersequence there are no parameter clashes: we may view this as a *local uniqueness* of parameters. However, the impact of this design choice is even more far-reaching: since parameters are stored globally, they will always have the same value in *all* possible supersequences (or in other words, the parameters are *globally unique*). This makes it exceptionally easy to set up multiple different supersequences in TopSpin: virtually all of the parameter values may simply be copied from a previous NOAH dataset.

One potential issue with this strategy is that TopSpin provides a finite number of named pulse widths (for example). Thus, there are only so many different parameters which can be stored in a global table before running into inevitable conflicts. A workaround would be to sacrifice the global uniqueness of each parameter, and only have it be unique within a given supersequence. Fortunately, this situation has not (yet) surfaced.*

Parameter descriptions

At the epilogue of the pulse programme, extra comments are added for every parameter present in the pulse programme. Most of these are purely textual, and appear in the TopSpin `ased` parameter setup screen; this naturally helps to make the pulse programmes as easy to use as possible. However, some of these comments have especial meaning: gradient amplitudes and shapes, for example, are specified in a way which allows them to be automatically populated using the `gppp` Python script in TopSpin. Furthermore, WaveMaker directives are also specified for some shaped pulses, allowing them to be created in an on-the-fly manner using the `wvm` command. This means that the user (generally) need not separately download and install a set of shaped pulses.

Module choice

One final issue which must be overcome is the fact that some NOAH modules may be implemented differently depending on the supersequence which it is being used in. The HMBC module described in § 4.1.3 is one such example: the form of the *zz*-filter depends on whether the HMBC module must retain $^{1}H^{C}$ and/or $^{1}H^{N}$ magnetisation for subsequent modules. Thus, in the NOAH-2 BS supersequence the *zz*-HMBC must be used, but in the NOAH-2 SB supersequence the 'original' HMBC without a *zz*-filter is preferable. Since they have different pulse programmes, each of these 'versions' of the HMBC are described by *separate* `NOAHModule` objects.

*The number of *pulse phases* in particular, though, is dangerously close to the maximum number of 32. In fact, the global uniqueness criterion is not really important for pulse phases, because—unlike, say, delays—pulse phases are hardcoded in the pulse programme, and cannot be copied from one dataset to another. So, if necessary, I could dispense with the global uniqueness for pulse phases, at the cost of some increased code complexity. I did briefly contemplate this possibility, but since I am at the end of my DPhil and am unlikely to add any new modules soon, this will remain a hypothetical—for now.

However, it is unlikely that the majority of users would want to manually configure the supersequence in such detail. Thus, the GENESIS web interface actually hides these different versions from the user, only showing one button labelled 'HMBC'. Under the hood, the correct version of the HMBC is automatically chosen based on what other modules the user has chosen (fig. 4.7).

fig:hmbc_flowchart

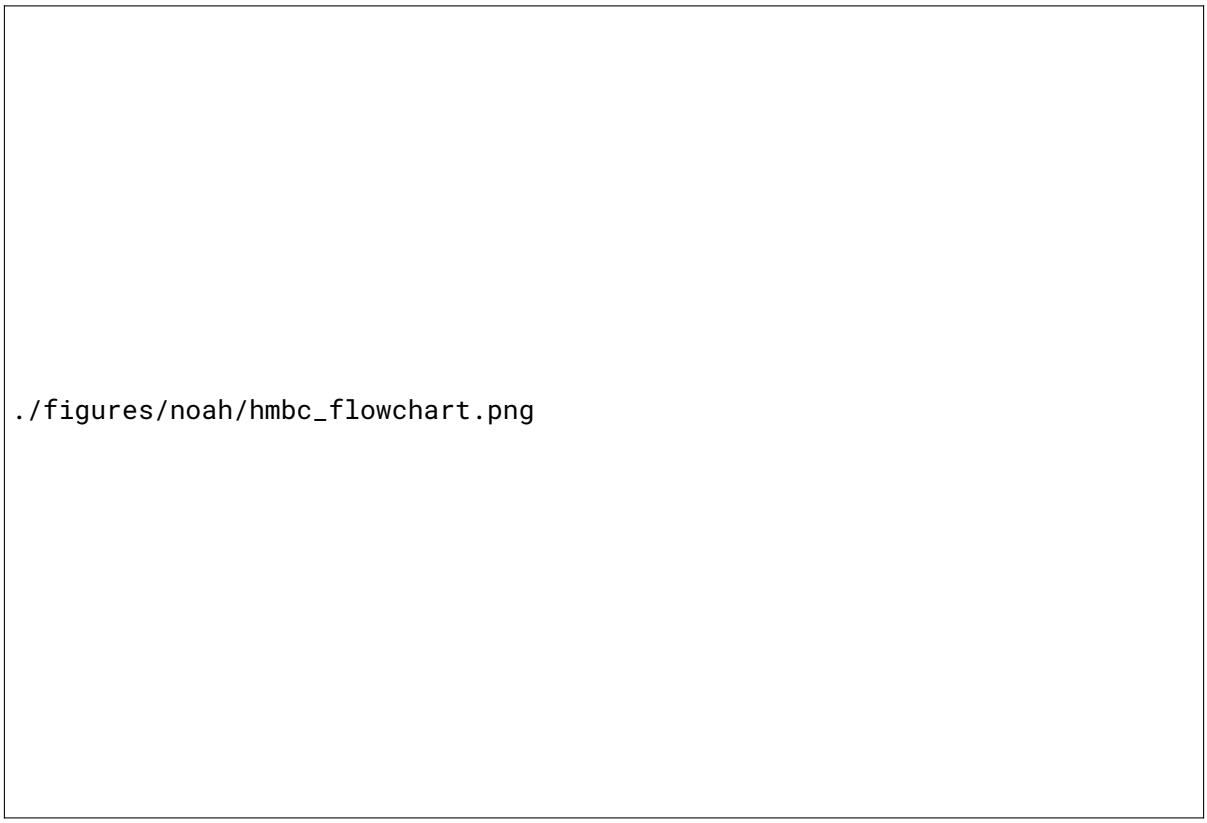

Figure 4.7: Flowchart showing how the correct 'version' of the HMBC module is determined when constructing a supersequence using GENESIS. When developer mode is on, the user directly chooses module codes corresponding to each version of the HMBC. When it is off, the appropriate version is chosen based on which other modules are present in the supersequence.

Should the user indeed desire to control the exact module used, the website also offers a 'developer mode' switch: turning this on allows the user to directly choose the desired module code. (Enabling developer mode also reveals a handful of extra modules which were used exclusively for my DPhil and are not generally of interest.)

Tests

One risk inherent in any NMR experiment is the possibility of causing spectrometer damage when executing malformed pulse programmes. To minimise the chances of this, each version of GENESIS is checked against a series of automatic tests before being released. The most im-

portant tests ensure that each module containing decoupling statements also turn off decoupling immediately after acquisition. On top of this, there are also a series of regression tests where (Some) supersequences are checked against those generated by previous versions: any differences in these are automatically flagged for review.

None of this can actually *stop* wrong pulse programmes from being written. For example, if a module are incorrectly programmed (which is still very easy), then any supersequence containing that module will not be fully functional. However, the inclusion of tests minimises the chance of creating faulty pulse programmes.

It should be mentioned that this is not a *new* problem which GENESIS introduces: errors in pulse programmes can arise equally easily (if not *even more easily*) when they are handwritten. There is no way to really circumvent this, except through careful inspection of the pulse programme prior to execution. The real difference with GENESIS is that users may be more likely to blindly use the pulse programmes it creates, without applying an equal amount of caution. The tests are therefore not meant to ensure perfection, but rather to avoid some of the worst consequences which may surface. Of course, it is also not possible for GENESIS to prevent users from setting up parameters incorrectly (e.g. overly long acquisition times).

Reproducibility

The final section of a GENESIS pulse programme consists of comments intended solely for reproducibility purposes. These comments indicate exactly which `NOAHModule` objects were used to create the pulse programme (these can be manually entered via developer mode), as well as a GENESIS *version number*. Since GENESIS has been updated with some regularity during my DPhil, each release is assigned a version number, which broadly follows the principles of *semantic versioning*. Old versions of GENESIS may be accessed by navigating to the specific URL `https://nmr-genesis.co.uk/X/Y/Z` for version `X.Y.Z`. Together, these two pieces of information allow all pulse programmes to be regenerated whenever necessary: this is important for ensuring that the spectra thus acquired are reproducible (as far as possible).

How smart is GENESIS?

Having written several pages of text about the *features* present in GENESIS, it is tempting to think that it is 'intelligent' in its design of pulse programmes. At various points in time, extensions to the concept have even been proposed: in GENESIS, the building blocks used for pulse programme construction are NOAH modules, but one could envision breaking up these into the smallest possible units of pulses, delays, gradients, and so on, and using something like GENESIS to construct *arbitrary* pulse programmes. This was even speculatively mentioned in the paper.

However, in truth, GENESIS is a long way from being able to do such things. In particular, it does not have any actual understanding of the Bruker pulse programming syntax: *almost* all of the pulse programme instructions are hardcoded as strings.* Thus, the creation of pulse programmes is not *truly* being done from the ground up: instead of 'combining pulse sequence elements', a more accurate description is that the *text* corresponding to different pulse sequence elements is being concatenated. There is actually a substantial amount of brute force involved. In a similar way, it is not possible for the automated tests to really check for 'correctness' of the pulse programmes.

Of course, it is hardly a trivial task to write something more sophisticated: I would need to construct abstract representations of each pulse sequence element, and functions which could transform these into actual pulse programme commands. I feel that I would need rather more knowledge in computer science, especially a course on compilers and/or programming language theory, to do this. However, this was something I would have really liked to do had I had more time!

4.2.3 Processing improvements

ah__genesis_processing

Finally, I touch on a few small improvements in processing NOAH data: these are not strictly made possible by the GENESIS website, but having a unified source for pulse programmes and processing scripts does make it substantially easier to propagate these developments.

AU processing scripts

When processing NOAH experiments, the first step is to split up the FIDs of different modules into different files: this is done by the `splitx_au` AU programme. However, after that is done, `splitx_au` *also* calls on auxiliary AU programmes to process each of the resulting datasets. Each module is associated with a specific auxiliary AU programme: for example, HSQC data is processed with `noah_hsqc`, COSY data with `noah_cosy`, and so on.

Previously, these auxiliary AU programmes had to be specified manually using the `USERP1` through `USERP5` processing parameters, which respectively apply to the first through fifth modules in a supersequence. Although this was a perfectly serviceable setup, I realised that it was a source of annoyance when running multiple different supersequences, as modules would often be processed incorrectly if the processing parameters were inadvertently copied. Even when just running a single supersequence, this was still an extra cognitive load, especially for users who may not have been familiar with NOAH experiments.

*There are several exceptions where some parameters (for example, loop counters in DIPSI mixing) are dynamically generated, mainly to avoid clashes between different parts of the supersequence.

Since the pulse programme specifies which modules are run, and the 'correct' processing parameters also depend on the modules, it stands to reason that the processing parameters can be encoded in the pulse programme itself. Thus, all GENESIS pulse programmes contain a line near the bottom specifying which AU programmes are to be used for each of the modules present. I also modified the `splitx_au` AU programme to parse the pulse programme for this extra information. Thus, the `USERP1` through `USERP5` parameters need no longer be specified, as long as a GENESIS pulse programme and a recent version of `splitx_au` are used. These parameters still serve a purpose, though; if they are non-empty, they will override the 'default' processing instructions found in the pulse programme. This maintains backwards compatibility with, for example, parameter sets which have been previously saved; it also allows advanced users to customise the processing, if so desired.

Non-uniform sampling

Another small improvement relates to the implementation of non-uniform sampling (NUS) in NOAH supersequences. Because the indirect dimension in NOAH pulse programmes is generated through explicit looping (listing 4.3), instead of the `mc` macro used in most 2D experiments, the standard NUS implementation in TopSpin cannot be used. Instead, one must explicitly define a list of t_1 increments to sample (stored as the `VCLIST` parameter). On top of this, the original NUS implementation[41] used a Python script (`noah_nus.py`) to modify the NOAH pulse programme such that it only sampled t_1 values from this list. This, however, necessitated storing two copies of the same pulse programme, one with NUS and one without.

There is no way to circumvent the requirement for the `VCLIST` parameter, but in GENESIS pulse programmes, I opted to implement NUS as an acquisition flag which could be toggled. This means that there is no need to store two versions of the same pulse programme, and also makes it easier to seamlessly switch between non-uniform and uniform sampling as desired.

Unfortunately, this change is slightly more problematic than the `splitx_au` change: this new NUS implementation is not backwards-compatible, so requires a new NUS setup script which I have called `noah_nus2.py`. This script cannot be used with old pulse programmes, and the old script cannot be used with GENESIS pulse programmes. Nevertheless, it does represent a real improvement over the previous implementation: the GENESIS website also helps to make the changeover as smooth as possible.*

*That said, there were still some bugs in the new NUS implementation right up until August 2022, so this change was not as smooth-sailing as I had hoped for.

4.3 Discussion of individual modules

sec:noah__modules

The GENESIS website makes it possible to easily implement and distribute entirely new modules, as well as updates to old modules: simply changing the underlying `NOAHModule` objects is sufficient to propagate changes to all supersequences generated using those modules. In this section, I discuss a number of new pulse sequence developments made in the course of my DPhil; all of these have been successfully implemented in GENESIS and are available to download.

4.3.1 ^{13}C sensitivity-enhanced HSQC

subsec:noah__sehsqc_c

^{13}C seHSQC

4.3.2 ^{15}N sensitivity-enhanced HSQC

subsec:noah__sehsqc_n

^{15}N seHSQC

4.3.3 HMQC

subsec:noah__hmqc

Suppression of wing artefacts (GENESIS paper)

4.3.4 HSQC-TOCSY

subsec:noah__hsqctocsy

HSQC + DIPSI + HSQC combos

Extension to HSQC-TOCSY

Cite ASAP work (Luy)

4.3.5 HSQC-COSY

subsec:noah__hsqccosy

Comparison of several versions of HSQC-COSY (JACS Au SI)

4.3.6 2DJ and PSYCHE

subsec:noah__2djpsyche

cnst37 scaling

SAPPHIRE

4.3.7 HMBC

subsec:noah__hmbc

The HMBC module is one which in fact does not fit perfectly into the NOAH principle of only exciting magnetisation which is needed. As described in § 4.1.3, the HMBC module should only

require magnetisation of protons which have long-range couplings to ^{13}C; however, it ends up exciting *all* ^{1}H$^{!C}$ magnetisation. This leads to sharply reduced, and also unbalanced, intensities of homonuclear modules which come later in the supersequences.

I made some early (and brief) attempts at devising a pulse sequence which sought to discriminate these two magnetisation components using a perfect echo.[47] However, this was quickly abandoned as it proved very difficult to *also* retain ^{1}H^{C} magnetisation. I do not claim here that it is impossible to come up with a pulse sequence which does this, but it is certainly not easy, and ultimately I turned my focus to improving (rather than replacing) the HMBC module.

Suppression of one-bond artefacts

One of the issues with the NOAH HMBC module was that there were an unusual amount of one-bond artefacts, which arise from ^{1}H^{C} magnetisation which is allowed to evolve during the pulse sequence. Generally, HMBC experiments seek to suppress this through the use of a low-pass J-filter (LPJF, see also § 3.4.7). The NOAH HMBC module *additionally* contains a *zz*-filter, which stores ^{1}H^{C} magnetisation along $+z$ before the LPJF. Thus, in theory, one-bond artefacts should be suppressed in the NOAH HMBC to an even greater extent.

However, this is not borne out: in some cases, the NOAH HMBC in fact has *more intense* one-bond artefacts when compared against a standard HMBC experiment (figs. 4.8a and 4.8c). Even performing an optimisation of the LPJF delays, as described in § 3.4.7, did not lead to any reduction in artefacts. I hypothesised instead that these artefacts arose from imperfect manipulation of ^{1}H^{C} magnetisation by the *zz*-filter.* In particular, any *antiphase* magnetisation (of the form I_xS_z or I_yS_z) generated after the *zz*-filter would be reconverted into in-phase I_x or I_y terms, which would not be destroyed by the LPJF. (The LPJF works based on the assumption that there is in-phase magnetisation at the beginning of it, which is true if the excitation element is just a ^{1}H 90° pulse.)

Such antiphase terms can be easily removed by the addition of a ^{13}C 90° pulse, which transforms them into a mixture of double- and zero-quantum terms: these are either unobservable, or can be efficiently dephased by CTP gradients. This technique is used in the CLIP-HSQC family of experiments,[48,49] as well as the LPJF itself. In this case, we simply need to add an additional ^{13}C 90° pulse at the end of the *zz*-filter: this pulse is highlighted in fig. 4.2b. This results in a striking reduction of the one-bond artefacts, as shown in fig. 4.8b. The suppression accomplished with the addition of this 90° pulse is superior to that in the standard HMBC (fig. 4.8c), and is comparable to a standard HMBC with a third-order LPJF (fig. 4.8d). Of course, the NOAH module—which by default uses a second-order LPJF—can also be 'upgraded' to use a third-order

*It would be nice to back this up with simulations, but I did not have the time to run these.

LPJF. In GENESIS pulse programmes, this can be done using the `-DLP3` acquisition flag (although the results were not evaluated here).

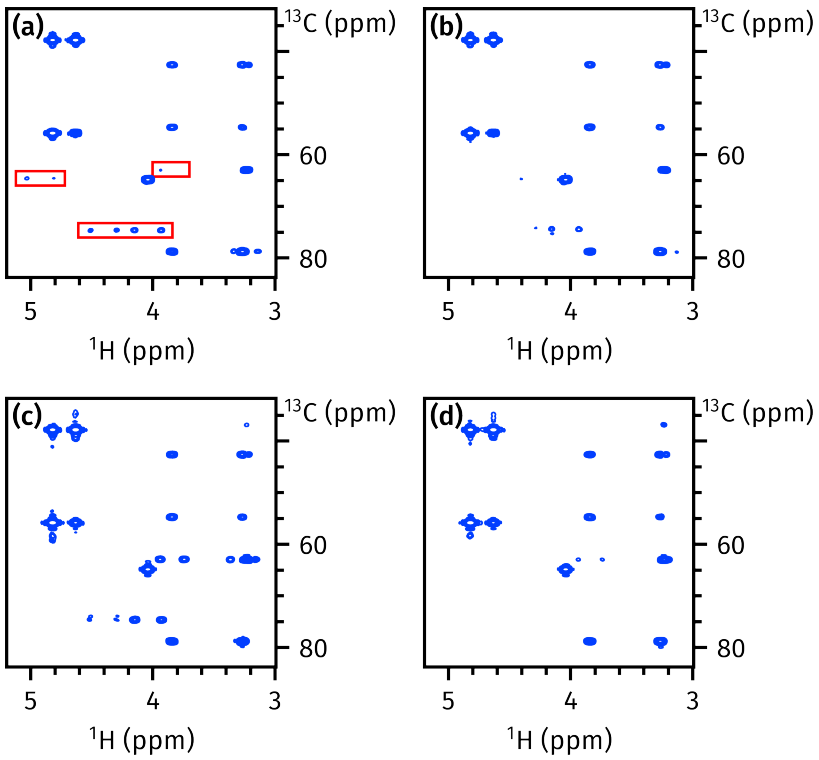

Figure 4.8: **(a)** NOAH *zz*-HMBC module without the additional 90° pulse. One-bond artefacts are highlighted in red. **(b)** NOAH *zz*-HMBC with the 90° pulse. **(c)** Standard library HMBC with a second-order LPJF. **(d)** Standard library HMBC with a third-order LPJF. *Data code:* `7A-210916`.

Gradient selection schemes

Another point which was investigated (but bore less fruit) was the gradient scheme used for CTP selection. The NOAH module, as shown in fig. 4.2b, uses a 'symmetric' scheme where two gradients of equal amplitude surround the t_1 period: this encoding is later decoded by a third gradient just prior to acquisition. However, other choices exist: for example, the Bruker standard library HMBC (derived from the work of Cicero et al.[50]) uses only two gradients in total, which have unequal amplitudes.

This gradient scheme cannot be directly used in a NOAH HMBC module, though. This is because the *zz*-filter element places $^{1}H^{C}$ magnetisation along the $+z$ axis just before the HMBC J-evolution delay (see fig. 4.2b). This magnetisation later experiences the ^{1}H 180° pulse in the middle of t_1, which means that an extra 180° pulse must be added at the very end of the sequence to finally return it to $+z$. It is necessary to ensure that there is at least one gradient placed after this 180° pulse to ensure proper CTP selection (in the 'symmetric' scheme of fig. 4.2b, this is fulfilled by the gradient g_2).

Figure 4.9: Alternative CTP gradient schemes investigated for the NOAH HMBC module. The coherences selected for during each gradient are indicated above each gradient, using the same notation for product operators as described in the *Preface*: the 'upper' term (e.g. + in ±) refers to the echo experiment, and the 'lower' term to the antiecho experiment. So, for example, +± refers to selection of I_+S_+ during the echo experiment and I_+S_- during the antiecho experiment. Gradient amplitudes are as described in the text. **(a)** 'Asymmetric scheme A', modified from the standard library sequence to include an additional 180° pulse and gradient. **(b)** 'Asymmetric scheme B', where the 180° pulse is shifted forward to the end of t_1. **(c)** 'Asymmetric scheme C', which modifies the *zz*-filter instead of using an extra 180° pulse. **(d)** The original 'symmetric' scheme (the same as in fig. 4.2b), placed here for convenience.

Using this knowledge, it is possible to construct several 'asymmetric' gradient schemes:

1. 'Scheme A' (fig. 4.9a) is modified from the Bruker standard library to include a 180° pulse and gradient at the end. The presence of an additional gradient means that there is a free parameter, here denoted as α, which can be used to control the relative amplitudes of these three CTP gradients. The gradient amplitudes are chosen as follows:

$$\text{echo:} \qquad g_1 = gc_1 \qquad g_2 = g \qquad g_3 = gc_2 \tag{4.6}$$ {eq:noah_hmbc_grads_bg

$$\text{antiecho:} \qquad g_1 = g \qquad g_2 = gc_1 \qquad g_3 = gc_2 \tag{4.7}$$ {eq:noah_hmbc_grads_bg

   where $c_1 = -\alpha(\gamma_H - \gamma_C)/(\gamma_H + \gamma_C)$ and $c_2 = (1-\alpha)(\gamma_H - \gamma_C)/\gamma_H$. In principle g is also a free parameter; for maximum suppression of artefacts I chose a relatively large value of 80%.

2. In 'Scheme B' (fig. 4.9b), the 180° pulse is shifted to immediately after t_1, before any of the CTP gradients have been applied. This means that there is no need for a third gradient, and the CTP gradient amplitudes can be directly taken from the standard library sequence:

$$\text{echo:} \qquad g_1 = g \qquad g_2 = gc \tag{4.8}$$ {eq:noah_hmbc_grads_bg

$$\text{antiecho:} \qquad g_1 = gc \qquad g_2 = g \tag{4.9}$$ {eq:noah_hmbc_grads_bg

   where $c = -(\gamma_H - \gamma_C)/(\gamma_H + \gamma_C)$ and $g = 80\%$.

3. 'Scheme C' (fig. 4.9c) simply does not add a 180° pulse, but instead modifies the phases of the zz-filter in order to place $^1H^C$ magnetisation along the $-z$ axis during the HMBC J-evolution delay. Here, the gradient amplitudes are the same as those in the standard library sequence as well as in scheme B.

It is of interest to note two limiting cases of scheme A: when $\alpha = (\gamma_H + \gamma_C)/(\gamma_H - \gamma_C) \approx 1.67$, we have that $g_1 : g_2 : g_3 = 1 : -1 : \pm 2\gamma_C/\gamma_H$, which mimics the original 'symmetric' scheme (fig. 4.9d); and when $\alpha = 1$, we have that $g_3 = 0$, i.e. a return to the two-gradient tactic of schemes B and C. In the tests which follow, I ran scheme A with $\alpha = 1.67$, $\alpha = 0.6$, and $\alpha = 0.3$.

All of the different HMBC versions above, plus the original 'symmetric' scheme in fig. 4.2b, were tested in the context of a NOAH-2 BS supersequence using the andrographolide sample (fig. 4.10). Since the HMBC module is the first module in this supersequence, the values here are an accurate reflection of their intrinsic sensitivities. As can be seen, there is not much at all which separates the different versions (outliers with $> 2\times$ 'sensitivity improvements' can be attributed to different J-modulation in the multiplet). The most sensitive of these is asymmetric scheme C, which may be explained by the fact that it has one fewer 180° pulse: however, this comes with an immediate drawback. Since scheme C places the $^1H^C$ magnetisation along $-z$ during the LPJF

fig:hmbc_grad_sens

Figure 4.10: Sensitivities of various asymmetric HMBC gradient schemes, as compared to the symmetric scheme in fig. 4.2b. Each dot indicates one crosspeak in the HMBC spectrum; the numbers in parentheses are the average over all peaks. *Data code:* `7A-211226`.

as well as the J-evolution delay Δ_{LR} (a total of ca. 70 ms), relaxation losses during this period lead to poorer retention of $^{1}H^{C}$ magnetisation for later modules, as shown by the decreased HSQC sensitivities in fig. 4.11. In contrast, all the other gradient schemes retain $^{1}H^{C}$ magnetisation equally well.

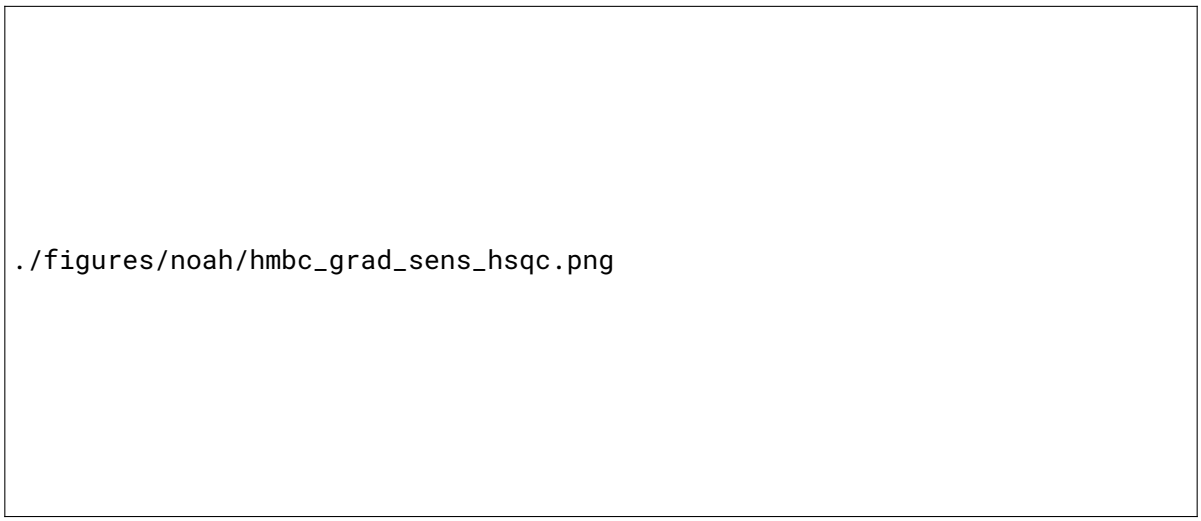

ig:hmbc_grad_sens_hsqc

Figure 4.11: Sensitivities of the HSQC module in a NOAH-2 BS supersequence, where the HMBC module is implemented using the gradient schemes of fig. 4.10. *Data code:* `7A-211226`.

The final point worth studying is the quality of the HMBC spectrum itself. To do this, we need to look at the actual spectra (fig. 4.12). For the most part, the spectra are all the same; however, there is a notable set of artefacts present in fig. 4.12b (scheme A with $\alpha = 1.67$) as well as fig. 4.12e

(scheme B), highlighted in red boxes. These artefacts occur at the frequencies

$$(\Omega_1, \Omega_2) = \left(\Omega_S \pm \frac{\Omega_I}{2}, \Omega_I\right), \tag{4.10}$$ {eq:hmbc_wing_artefact

and are in fact 'wing' artefacts similar to that observed in other modules insert reference. In this case, they arise due to imperfect refocusing of the ^{1}H chemical shift during t_1: specifically, whenever $I_z S_\pm$ terms are present during the second half of t_1. Extra evidence for the origin of these artefacts comes from the observation that when the 180° pulse in the middle of t_1 is phase cycled, the artefacts are removed. In a standard HMBC, these terms would not be detected in the final FID; however, in this case, the addition of an extra 180° pulse after t_1 provides an opportunity for these to be converted back into observable spin-I magnetisation (through off-resonance effects or miscalibration).

The poorer performance may therefore be understood as follows: when scheme A is acquired with $\alpha = 1.67$, the gradients g_1 and g_2 have equal and opposite amplitudes, and so do not enforce any coherence selection on spin I during the second half of t_1. Likewise, scheme B contains no gradients during the second half of t_1.

The characteristics of these gradient schemes are summarised in table 4.3. As can be seen, the 'best' schemes are either the original symmetric scheme, or asymmetric scheme A with $\alpha \neq 1.67$. However, there is not much difference between these: it is not clear whether the improvement in sensitivity is reproducible across a wide range of samples, and in any case, the gains are extremely marginal.

Gradient scheme	HMBC sensitivity	HSQC sensitivity	Wing artefacts
Symmetric	1	1	No
Asymmetric A, $\alpha = 1.67$	1.05	0.99	Yes
Asymmetric A, $\alpha = 0.6$	1.04	0.99	No
Asymmetric A, $\alpha = 0.3$	1.05	0.99	No
Asymmetric B	1.06	1.01	Yes
Asymmetric C	1.09	0.71	No

tbl:hmbc_grads

Table 4.3: Comparison of HMBC gradient schemes discussed in this section: the data are a summary of figs. 4.10 to 4.12.

Other artefacts

It has been established that the HMBC module (and supersequences containing it) are not fully ideal in terms of magnetisation preservation. However, there are also some other curious phenomena which have not been fully described in the literature. One of these is the presence of *inverted peaks* in the homonuclear X module(s) in a NOAH-3 BSX supersequence: this is

Figure 4.12: HMBC spectra acquired with the gradient schemes of fig. 4.10. Extra 'wing' artefacts present in two of the spectra (asymmetric scheme A with $\alpha = 1.67$, **(b)**, and asymmetric scheme B, **(e)**) are highlighted in red boxes.

illustrated in fig. 4.13a with the CLIP-COSY module (X = C^c). It is not clear why this occurs, because the HMBC module (and the gradients which follow) should dephase all $^1H^{!C}$ magnetisation. Although this leads to reduced sensitivity in the homonuclear module, in that the signal derives from polarisation which has recovered during the preceding FIDs, it is not clear why this polarisation should be *negative*. One clue lies in the fact that these peaks are very sensitive to the ^1H 90° pulse width: simply changing this by 0.5 µs is sufficient to restore the correct signal sign (fig. 4.13b).

The modules placed between the HMBC and the homonuclear module also play an important role. When *two* HSQC modules are used, i.e. a NOAH-4 $BSSC^c$ supersequence (using $f = 0.7$ as described in § 4.3.4—although this is unlikely to matter), the negative peaks are no longer observed (fig. 4.13c). In fact, having *no modules* between the HMBC and the homonuclear module is also (at least sometimes) acceptable: a separate set of data shows that the inverted peaks in an NOAH-3 BS^+C^c experiment are not seen in a NOAH-3 S^+BC^c supersequence (figs. 4.14a and 4.14b). The use of ASAP mixing just before the homonuclear module does not

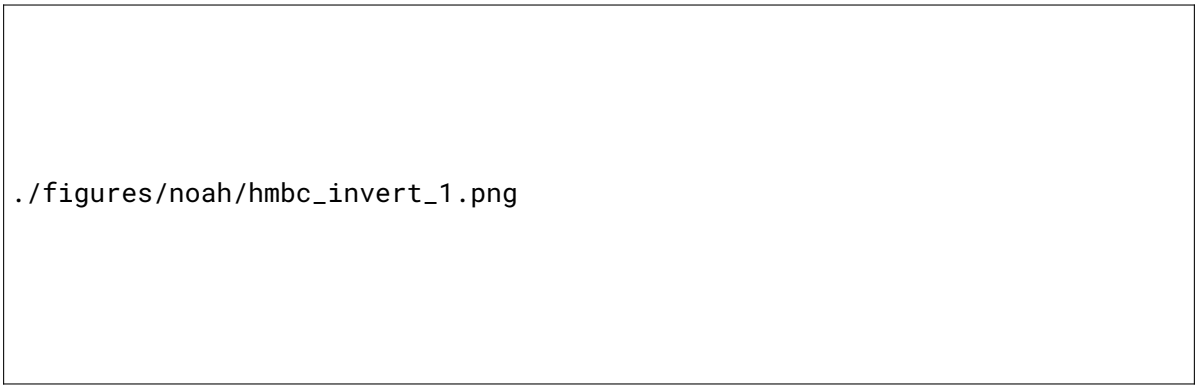

Figure 4.13: **(a)** CLIP-COSY from a NOAH-3 BSC^{c} supersequence, acquired with a ^{1}H 90° pulse width of 11.28 µs (this value was obtained using the POISE calibration described in § 3.4.1). An inverted peak is visible at 2.25 ppm. **(b)** The same, but acquired using a 90° pulse width of 11.78 µs. **(c)** CLIP-COSY from a NOAH-4 BSSC^{c} supersequence. The 90° pulse width was 11.28 µs, the same as in (a). *Data code:* `7Z-220214`.

remedy this (figs. 4.14c and 4.14d). Unfortunately, a good explanation for these artefacts has remained elusive.

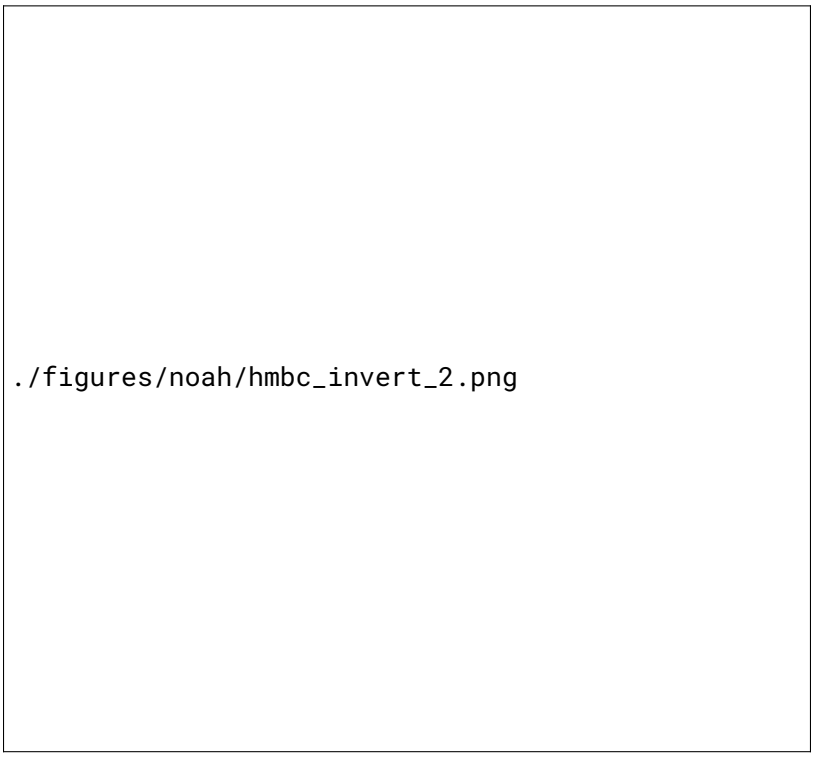

Figure 4.14: **(a)** CLIP-COSY from a NOAH-3 BS^{+}C^{c} supersequence. An inverted diagonal peak can be seen at 6.6 ppm. **(b)** From a NOAH-3 S^{+}BC^{c} supersequence. **(c)**–**(d)** The same as (a) and (b), but with 40 ms ASAP mixing placed just before the CLIP-COSY module. *Data code:* `7A-211227`.

^{15}N HMBC module

The entirety of this section has—until now—been devoted to the ^{13}C HMBC module. However, the techniques used in constructing this, including the implementation of the *zz*-filter, are equally applicable to a ^{15}N HMBC. For simplicity, the NOAH ^{15}N HMBC module uses a first-order LPJF (since $^{1}J_{\mathrm{NH}}$ pairs are less common); this may be omitted if desired. To minimise the number of pulses, a simple magnitude-mode version of the HMBC is used (fig. 4.15). The implementation of this module within supersequences is discussed in greater detail within the context of *generalised supersequences*, in REF.

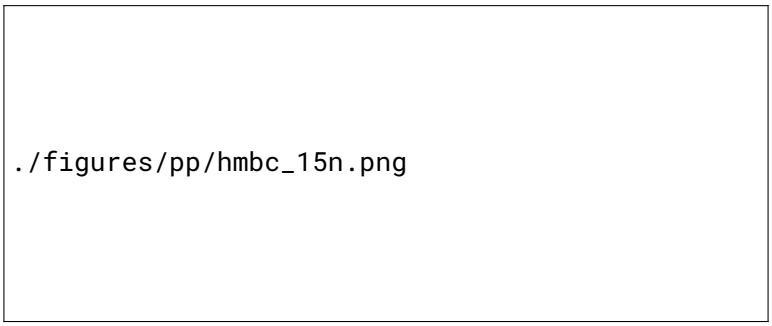

fig:noah_15n_hmbc

Figure 4.15: NOAH ^{15}N HMBC module. The *zz*-filter can be implemented as necessary in the same way as for the ^{13}C HMBC module (a final ^{1}H 180° pulse may also be required, but is not shown here). Delays are set as follows: $\Delta_{\mathrm{N}} = 1/(2 \cdot {}^{1}J_{\mathrm{NH}})$; $\Delta_{\mathrm{LR,N}} = 1/(2 \cdot {}^{n}J_{\mathrm{NH}})$. Phase cycling is performed using $\phi_1 = \phi_{\mathrm{rec}} = (x, -x)$ and $\phi_2 = (x, x, -x, -x)$. Gradient amplitudes are $(g_1, g_2, g_3, g_4) = (5\%, 70\%, 30\%, 50.1\%)$.

4.3.8 ADEQUATE

subsec:noah__adequate

Recent stuff.

4.4 Solvent suppression in NOAH

sec:noah__solvsupp

Solvent suppression is one of the most important aspects of modern NMR, and has been incorporated into a large number of experiments. It is not a particularly difficult task to implement some basic solvent suppression techniques in NOAH supersequences, as will be described in this section. All suppression techniques shown here can be enabled via acquisition flags (the TopSpin `ZGOPTNS` parameter); this means that there is no need to switch pulse sequences.

4.4.1 Presaturation

:noah__solvsupp_presat

A simple first step is to implement simple presaturation of the solvent resonance during the recovery delay of the sequence. This often provides excellent suppression in the first module

in a supersequence, and to a lesser extent, later modules (as the solvent magnetisation recovers during acquisition periods).

Presaturation is also included during long delays, in particular mixing times in NOESY experiments. The use of presaturation during the HMBC J-evolution delay was also tested, but was found to be generally unnecessary, especially since the HMBC module is typically placed first in supersequences.

4.4.2 Intrinsic suppression

ah__solvsupp_intrinsic

A number of NOAH modules in fact come with an *intrinsic* form of solvent suppression, in that they return $^{1}H^{!X}$ magnetisation (including that of solvents) to the $+z$ axis at the end of the module. This is generally true of many of the HSQC-based NOAH modules, which seek to only sample $^{1}H^{X}$ magnetisation pool. Thus, these modules already have far better solvent suppression properties compared to standard library sequences: there is no need for further modification.

For these sequences, it is interesting to go one step further and to see how the solvent suppression varies with transmitter offset. This is less relevant if the solvent is just water (in which case it suffices to put the water peak on resonance), but may be important for samples in protonated solvents or mixtures thereof. I tested this by recording the first increment of the NOAH HSQC and seHSQC modules on an aqueous sample of sucrose, and integrating the water peak. The results (fig. 4.16) indicate that the HSQC module provides the best suppression across a range of offsets; of the two seHSQC modules, seHSQC1 provides more uniform suppression, whereas seHSQC2 has some regions ('spikes') where suppression is poorer than average.

It is not surprising that the more complicated seHSQC sequences have slightly poorer suppression: there are substantially more pulses involved which lead to cumulative errors, especially for peaks which are further away from resonance. However, it is not entirely clear why seHSQC2 has such large spikes. Some further investigation showed that the poorer suppression partly arises from imperfect cancellation of the water signal by phase cycling. This is, however, not a full explanation; it merely replaces one mystery with another. Nevertheless, it should be reiterated that all of these sequences still provide excellent water suppression. The standard library seHSQC sequences, for example, do not even come close to this level of suppression (although these do dephase water magnetisation prior to acquisition, radiation damping still leads to a very large signal being detected).

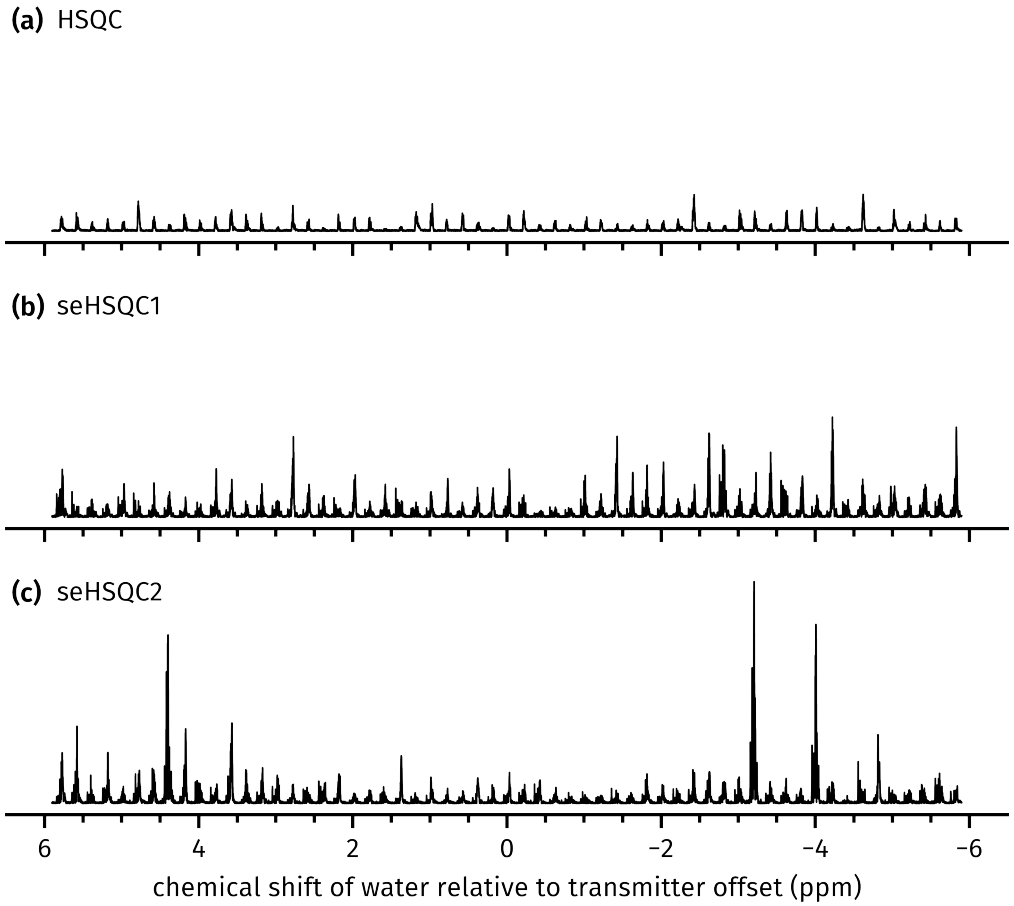

Figure 4.16: Residual water peaks observed in the first increment of NOAH HSQC and seHSQC modules, as a function of transmitter offset. The *y*-axes of the three subplots are the same. **(a)** HSQC module. **(b)** seHSQC1 module. **(c)** seHSQC2 module. *Data code:* `7S-201014`.

4.4.3 Excitation sculpting

Since solvent suppression in HMBC and HSQC-type modules can be adequately accomplished through presaturation and intrinsic suppression, it remains to consider the suppression in homonuclear modules. These modules invariably occur at the end of supersequences, and thus almost any form of solvent suppression can be used: there is no need to consider how magnetisation needs to be preserved for other modules.

In practice, I chose to implement excitation sculpting[51] (ES) just prior to acquisition: the refocusing element chosen was a combination of a selective 180° sinc pulse and a hard 180° pulse. This worked perfectly for almost all of the homonuclear modules used in NOAH supersequences, with only a few adjustments needed, e.g. for the PSYCHE modules to ensure that chemical shifts and J-couplings evolved for the correct amount of time.

The case of the 'double' COSY + X homonuclear modules, however, proved to be more intricate.

This is illustrated here using X = TOCSY, but the considerations below are equally applicable to X = NOESY or ROESY. It is tempting to simply place ES blocks prior to both FIDs: in the COSY module, this dephases transverse solvent magnetisation as desired, and (in principle) should leave longitudinal magnetisation untouched, meaning that the TOCSY module which later consumes this should be unaffected.

However, this is not totally true. *Inside* the bandwidth of the selective 180° pulse, any longitudinal magnetisation experiences an 720° rotation; and *outside* of the bandwidth, it experiences a 360° rotation. However, *between* these two extremes, there is a crossover point where longitudinal magnetisation is sent into the transverse plane and subsequently dephased by gradients. These lead to nulls in fig. 4.17b, and peaks which fall within this range will be lost in the TOCSY module. This is visible in the spectra of fig. 4.18: although the water suppression obtained using this 'double ES' scheme is better, several peaks in the TOCSY spectrum have disappeared, because they fall precisely into these nulls. It proves better to omit the ES in the COSY module: an adequate degree of water suppression in the COSY can still be attained thanks to the use of presaturation.

./figures/noah/double_es_sim.png

fig:noah__double_es_sim

Figure 4.17: Simulations showing the proportion of magnetisation retained by the excitation sculpting block (using a 2 ms sinc pulse). **(a)** Retention of transverse magnetisation: this was obtained by simulating the spectrum of a 90°–ES–detect pulse sequence. **(b)** Retention of longitudinal magnetisation: this was obtained using an ES–90°–detect pulse sequence.

Of course, it may well be that *no* peaks fall within this null, and thus the better solvent suppression may be obtained at no cost. This was the case when the experiments in fig. 4.18 were reacquired on a 700 MHz spectrometer; or when the sinc pulse was lengthened to 4 ms. However, such fortuitousness cannot always be relied on.

4.5 Parallel and generalised NOAH supersequences

sec:noah__parallel

Blah.

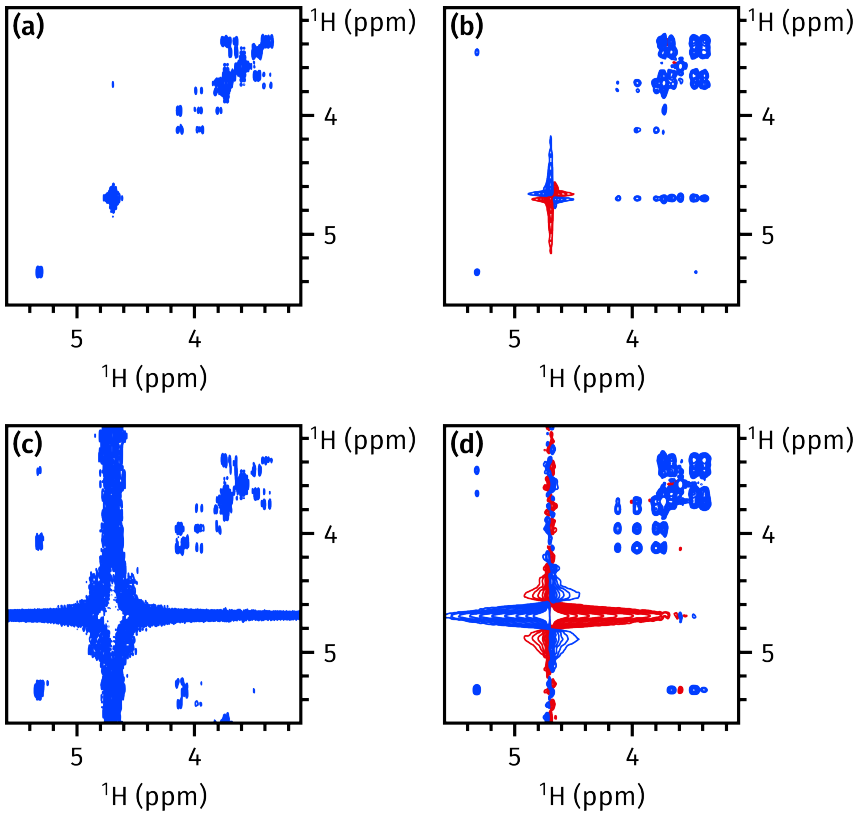

Figure 4.18: **(a)**–**(b)** COSY and TOCSY spectra obtained from a NOAH-3 SCT supersequence where excitation sculpting was placed before both the COSY and TOCSY FIDs. Although the water suppression is better, some peaks in the TOCSY module are lost. **(c)**–**(d)** The same, except that excitation sculpting was applied only in the TOCSY module. For all spectra shown here, presaturation of the water resonance was applied during the recovery delay. *Data code:* `4S-211105`.

4.6 References

Yong2021JMR (1) Yong, J. R. J.; Hansen, A. L.; Kupče, Ē.; Claridge, T. D. W. Increasing sensitivity and versatility in NMR supersequences with new HSQC-based modules. *J. Magn. Reson.* **2021**, *329*, 107027, DOI: 10.1016/j.jmr.2021.107027.

Kupce2021JACSA (2) Kupče, Ē.; Yong, J. R. J.; Widmalm, G.; Claridge, T. D. W. Parallel NMR Supersequences: Ten Spectra in a Single Measurement. *JACS Au* **2021**, *1*, 1892–1897, DOI: 10.1021/jacsau.1c00423.

Yong2022AC (3) Yong, J. R. J.; Kupče, Ē.; Claridge, T. D. W. Modular Pulse Program Generation for NMR Supersequences. *Anal. Chem.* **2022**, *94*, 2271–2278, DOI: 10.1021/acs.analchem.1c04964.

Yong2022_ABBS (4) Yong, J. R. J.; Kupče, Ē.; Claridge, T. D. W. Uniting Low- and High-Sensitivity Experiments through Generalised NMR Supersequences. **2022**, manuscript in preparation.

Kupce2021NRMP (5) Kupče, Ē.; Frydman, L.; Webb, A. G.; Yong, J. R. J.; Claridge, T. D. W. Parallel nuclear magnetic resonance spectroscopy. *Nat. Rev. Methods Primers* **2021**, *1*, No. 27, DOI: 10.1038/s43586-021-00024-3.

Yong2022RSCBook (6) Yong, J. R. J.; Kupče, Ē.; Claridge, T. D. W. In *Fast 2D solution-state NMR: concepts and applications*, Giraudeau, P., Dumez, J.-N., Eds., forthcoming, 2022.

Barna1987JMR (7) Barna, J. C. J.; Laue, E. D.; Mayger, M. R.; Skilling, J.; Worrall, S. J. P. Exponential sampling, an alternative method for sampling in two-dimensional NMR experiments. *J. Magn. Reson.* **1987**, *73*, 69–77, DOI: 10.1016/0022-2364(87)90225-3.

Kazimierczuk2010PNMRS (8) Kazimierczuk, K.; Stanek, J.; Zawadzka-Kazimierczuk, A.; Koźmiński, W. Random sampling in multidimensional NMR spectroscopy. *Prog. Nucl. Magn. Reson. Spectrosc.* **2010**, *57*, 420–434, DOI: 10.1016/j.pnmrs.2010.07.002.

Mobli2014PNMRS (9) Mobli, M.; Hoch, J. C. Nonuniform sampling and non-Fourier signal processing methods in multidimensional NMR. *Prog. Nucl. Magn. Reson. Spectrosc.* **2014**, *83*, 21–41, DOI: 10.1016/j.pnmrs.2014.09.002.

Kazimierczuk2015MRC (10) Kazimierczuk, K.; Orekhov, V. Non-uniform sampling: post-Fourier era of NMR data collection and processing. *Magn. Reson. Chem.* **2015**, *53*, 921–926, DOI: 10.1002/mrc.4284.

eSunninghausen2014JACS (11) Schulze-Sünninghausen, D.; Becker, J.; Luy, B. Rapid Heteronuclear Single Quantum Correlation NMR Spectra at Natural Abundance. *J. Am. Chem. Soc.* **2014**, *136*, 1242–1245, DOI: 10.1021/ja411588d.

Schanda2006JACS (12) Schanda, P.; Van Melckebeke, H.; Brutscher, B. Speeding Up Three-Dimensional Protein NMR Experiments to a Few Minutes. *J. Am. Chem. Soc.* **2006**, *128*, 9042–9043, DOI: 10.1021/ja062025p.

Kupce2007MRC (13) Kupče, Ē.; Freeman, R. Fast multidimensional NMR by polarization sharing. *Magn. Reson. Chem.* **2007**, *45*, 2–4, DOI: 10.1002/mrc.1931.

Schanda2009PNMRS (14) Schanda, P. Fast-pulsing longitudinal relaxation optimized techniques: Enriching the toolbox of fast biomolecular NMR spectroscopy. *Prog. Nucl. Magn. Reson. Spectrosc.* **2009**, *55*, 238–265, DOI: 10.1016/j.pnmrs.2009.05.002.

Frydman2002PNASUSA (15) Frydman, L.; Scherf, T.; Lupulescu, A. The acquisition of multidimensional NMR spectra within a single scan. *Proc. Natl. Acad. Sci. U. S. A.* **2002**, *99*, 15858–15862, DOI: 10.1073/pnas.252644399.

Pelupessy2003JACS (16) Pelupessy, P. Adiabatic Single Scan Two-Dimensional NMR Spectrocopy. *J. Am. Chem. Soc.* **2003**, *125*, 12345–12350, DOI: 10.1021/ja034958g.

Frydman2003JACS (17) Frydman, L.; Lupulescu, A.; Scherf, T. Principles and Features of Single-Scan Two-Dimensional NMR Spectroscopy. *J. Am. Chem. Soc.* **2003**, *125*, 9204–9217, DOI: 10.1021/ja030055b.

Tal2010PNMRS (18) Tal, A.; Frydman, L. Single-scan multidimensional magnetic resonance. *Prog. Nucl. Magn. Reson. Spectrosc.* **2010**, *57*, 241–292, DOI: 10.1016/j.pnmrs.2010.04.001.

Gouilleux2018ARNMRS (19) Gouilleux, B.; Rouger, L.; Giraudeau, P. Ultrafast 2D NMR: Methods and Applications. *Annu. Rep. NMR Spectrosc.* **2018**, 75–144, DOI: 10.1016/bs.arnmr.2017.08.003.

Kupce2003JMR (20) Kupče, Ē.; Freeman, R. Two-dimensional Hadamard spectroscopy. *J. Magn. Reson.* **2003**, *162*, 300–310, DOI: 10.1016/s1090-7807(02)00196-9.

Kupce2003PNMRS (21) Kupče, E.; Nishida, T.; Freeman, R. Hadamard NMR spectroscopy. *Prog. Nucl. Magn. Reson. Spectrosc.* **2003**, *42*, 95–122, DOI: 10.1016/s0079-6565(03)00022-0.

Jeannerat2000MRC (22) Jeannerat, D. High resolution in the indirectly detected dimension exploiting the processing of folded spectra. *Magn. Reson. Chem.* **2000**, *38*, 415–422, DOI: 10.1002/1097-458x(200006)38:6<415::aid-mrc665>3.0.co;2-u.

Bermel2009JACS (23) Bermel, W.; Bertini, I.; Felli, I. C.; Pierattelli, R. Speeding Up ^{13}C Direct Detection Biomolecular NMR Spectroscopy. *J. Am. Chem. Soc.* **2009**, *131*, 15339–15345, DOI: 10.1021/ja9058525.

Njock2010C (24) Njock, G. B. B.; Pegnyemb, D. E.; Bartholomeusz, T. A.; Christen, P.; Vitorge, B.; Nuzillard, J.-M.; Shivapurkar, R.; Foroozandeh, M.; Jeannerat, D. Spectral Aliasing: A Super Zoom for 2D-NMR Spectra. Principles and Applications. *Chimia* **2010**, *64*, 235, DOI: 10.2533/chimia.2010.235.

Nolis2007ACIE (25) Nolis, P.; Pérez-Trujillo, M.; Parella, T. Multiple FID Acquisition of Complementary HMBC Data. *Angew. Chem. Int. Ed.* **2007**, *46*, 7495–7497, DOI: 10.1002/anie.200702258.

Parella2010CMR (26) Parella, T.; Nolis, P. Time-shared NMR experiments. *Concepts Magn. Reson.* **2010**, *36A*, 1–23, DOI: 10.1002/cmr.a.20150.

Kupce2006JACS (27) Kupče, Ē.; Freeman, R.; John, B. K. Parallel Acquisition of Two-Dimensional NMR Spectra of Several Nuclear Species. *J. Am. Chem. Soc.* **2006**, *128*, 9606–9607, DOI: 10.1021/ja0634876.

Kupce2008JACS (28) Kupče, Ē.; Freeman, R. Molecular Structure from a Single NMR Experiment. *J. Am. Chem. Soc.* **2008**, *130*, 10788–10792, DOI: 10.1021/ja8036492.

Kovacs2016MRC (29) Kovacs, H.; Kupče, Ē. Parallel NMR spectroscopy with simultaneous detection of1H and19F nuclei. *Magn. Reson. Chem.* **2016**, *54*, 544–560, DOI: 10.1002/mrc.4428.

Kupce2017ACIE (30) Kupče, Ē.; Claridge, T. D. W. NOAH: NMR Supersequences for Small Molecule Analysis and Structure Elucidation. *Angew. Chem. Int. Ed.* **2017**, *56*, 11779–11783, DOI: 10.1002/anie.201705506.

Kupce2021PNMRS (31) Kupče, Ē.; Mote, K. R.; Webb, A.; Madhu, P. K.; Claridge, T. D. W. Multiplexing experiments in NMR and multi-nuclear MRI. *Prog. Nucl. Magn. Reson. Spectrosc.* **2021**, *124–125*, 1–56, DOI: 10.1016/j.pnmrs.2021.03.001.

Nagy2019CC (32) Nagy, T. M.; Gyöngyösi, T.; Kövér, K. E.; Sørensen, O. W. BANGO SEA XLOC/HMBC–H2OBC: complete heteronuclear correlation within minutes from one NMR pulse sequence. *Chem. Commun.* **2019**, *55*, 12208–12211, DOI: 10.1039/c9cc06253j.

Nagy2020JMR (33) Nagy, T. M.; Kövér, K. E.; Sørensen, O. W. Double and adiabatic BANGO for concatenating two NMR experiments relying on the same pool of magnetization. *J. Magn. Reson.* **2020**, *316*, 106767, DOI: 10.1016/j.jmr.2020.106767.

Nagy2021ACIE (34) Nagy, T. M.; Kövér, K. E.; Sørensen, O. W. NORD: NO Relaxation Delay NMR Spectroscopy. *Angew. Chem. Int. Ed.* **2021**, *60*, 13587–13590, DOI: 10.1002/anie.202102487.

Timari2022CC (35) Timári, I.; Nagy, T. M.; Kövér, K. E.; Sørensen, O. W. Synergy and sensitivity-balance in concatenating experiments in NO relaxation delay NMR (NORD). *Chem. Commun.* **2022**, *58*, 2516–2519, DOI: 10.1039/d1cc06663c.

Orts2018M (36) Orts, J.; Gossert, A. D. Structure determination of protein-ligand complexes by NMR in solution. *Methods* **2018**, *138-139*, 3–25, DOI: 10.1016/j.ymeth.2018.01.019.

zeSunninghausen2017JMR (37) Schulze-Sünninghausen, D.; Becker, J.; Koos, M. R. M.; Luy, B. Improvements, extensions, and practical aspects of rapid ASAP-HSQC and ALSOFAST-HSQC pulse sequences for studying small molecules at natural abundance. *J. Magn. Reson.* **2017**, *281*, 151–161, DOI: 10.1016/j.jmr.2017.05.012.

Vitorge2010JMR (38) Vitorge, B.; Bodenhausen, G.; Pelupessy, P. Speeding up nuclear magnetic resonance spectroscopy by the use of SMAll Recovery Times – SMART NMR. *J. Magn. Reson.* **2010**, *207*, 149–152, DOI: 10.1016/j.jmr.2010.07.017.

Shaw1996JMRSA (39) Shaw, A. A.; Salaun, C.; Dauphin, J.-F.; Ancian, B. Artifact-Free PFG-Enhanced Double-Quantum-Filtered COSY Experiments. *J. Magn. Reson., Ser. A* **1996**, *120*, 110–115, DOI: 10.1006/jmra.1996.0105.

Howe2014MRC (40) Howe, P. W. A. Rapid pulsing artefacts in pulsed-field gradient double-quantum filtered COSY spectra. *Magn. Reson. Chem.* **2014**, *52*, 329–332, DOI: 10.1002/mrc.4060.

Claridge2019MRC (41) Claridge, T. D. W.; Mayzel, M.; Kupče, Ē. Triplet NOAH supersequences optimised for small molecule structure characterisation. *Magn. Reson. Chem.* **2019**, *57*, 946–952, DOI: 10.1002/mrc.4887.

Haasnoot1984JMR (42) Haasnoot, C. A. G.; van de Ven, F. J. M.; Hilbers, C. W. COCONOSY. Combination of 2D correlated and 2D nuclear overhauser enhancement spectroscopy in a single experiment. *J. Magn. Reson.* **1984**, *56*, 343–349, DOI: 10.1016/0022-2364(84)90114-8.

Gurevich1984JMR (43) Gurevich, A. Z.; Barsukov, I. L.; Arseniev, A. S.; Bystrov, V. F. Combined COSY-NOESY experiment. *J. Magn. Reson.* **1984**, *56*, 471–478, DOI: 10.1016/0022-2364(84)90311-1.

Nolis2019MRC (44) Nolis, P.; Parella, T. Practical aspects of the simultaneous collection of COSY and TOCSY spectra. *Magn. Reson. Chem.* **2019**, *57*, S85–S94, DOI: 10.1002/mrc.4835.

Kupce2018CC (45) Kupče, Ē.; Claridge, T. D. W. Molecular structure from a single NMR supersequence. *Chem. Commun.* **2018**, *54*, 7139–7142, DOI: 10.1039/c8cc03296c.

Kupce2019JMR (46) Kupče, Ē.; Claridge, T. D. W. New NOAH modules for structure elucidation at natural isotopic abundance. *J. Magn. Reson.* **2019**, *307*, 106568, DOI: 10.1016/j.jmr.2019.106568.

Parella2019MRC (47) Parella, T. Towards perfect NMR: Spin-echo versus perfect-echo building blocks. *Magn. Reson. Chem.* **2019**, *57*, 13–29, DOI: 10.1002/mrc.4776.

Enthart2008JMR (48) Enthart, A.; Freudenberger, J. C.; Furrer, J.; Kessler, H.; Luy, B. The CLIP/CLAP-HSQC: Pure absorptive spectra for the measurement of one-bond couplings. *J. Magn. Reson.* **2008**, *192*, 314–322, DOI: 10.1016/j.jmr.2008.03.009.

Gyongyosi2021AC (49) Gyöngyösi, T.; Timári, I.; Sinnaeve, D.; Luy, B.; Kövér, K. E. Expedited Nuclear Magnetic Resonance Assignment of Small- to Medium-Sized Molecules with Improved HSQC–CLIP–COSY Experiments. *Anal. Chem.* **2021**, *93*, 3096–3102, DOI: 10.1021/acs.analchem.0c04124.

Cicero2001JMR (50) Cicero, D. O.; Barbato, G.; Bazzo, R. Sensitivity Enhancement of a Two-Dimensional Experiment for the Measurement of Heteronuclear Long-Range Coupling Constants, by a New Scheme of Coherence Selection by Gradients. *J. Magn. Reson.* **2001**, *148*, 209–213, DOI: 10.1006/jmre.2000.2234.

Hwang1995JMRSA (51) Hwang, T. L.; Shaka, A. J. Water Suppression That Works. Excitation Sculpting Using Arbitrary Wave-Forms and Pulsed-Field Gradients. *J. Magn. Reson., Ser. A* **1995**, *112*, 275–279, DOI: 10.1006/jmra.1995.1047.

refsection:5